Fluid-metasomatized mantle beneath the Ouachita belt of southern Laurentia: Fate of lithospheric mantle in a continental orogenic belt

H.P. Young[1,*] and C.-T.A. Lee[1]
[1]DEPARTMENT OF EARTH SCIENCE, RICE UNIVERSITY, HOUSTON, TEXAS 77005, USA

ABSTRACT

The nature and history of the cratonic lithosphere beneath the southern margin of Laurentia are poorly understood due to the paucity of basement exposure in the Gulf Coast region. One place where we are afforded the opportunity to study the deep lithosphere of southern Laurentia is within the Balcones igneous province of Texas. Mantle xenoliths occur in Late Cretaceous alkali basaltic magmas erupted through the remnants of the Appalachian-Ouachita structural belt. Geochemical signatures in the form of enrichments in fluid-mobile trace elements (e.g., La) relative to fluid-immobile trace elements (e.g., Nb) are preserved in these mantle xenoliths. We interpret these signatures to represent metasomatism by subduction-related fluids, suggesting that the mantle xenoliths represent fragments of continental lithospheric mantle that served as the upper plate during a convergent episode. These xenoliths may thus represent fragments of Laurentian lithospheric mantle that were stabilized by collisional processes during the continent-continent collisions associated with the Grenville orogeny and subsequent Paleozoic orogenies. These observations suggest that some of the original continental lithosphere was preserved beneath the orogenic belt during continent-continent collision and did not undergo wholesale removal or delamination. Alternatively, the fluid signatures may have been caused by Farallon flat-slab hydration of the overriding lithosphere, but such a scenario seems unlikely because flat subduction is thought to have culminated in the early Cenozoic and hence after the eruption of these xenoliths.

LITHOSPHERE; v. 1; no. 6; p. 370–383. doi: 10.1130/L72.1

INTRODUCTION

The southern margin of the Laurentian craton has experienced orogeny in both the Proterozoic (Grenville) and Paleozoic (Ouachita) (Hatcher, 1989). Southern Laurentia has not been central in plate reconstructions, mainly due to a lack of basement exposure. However, a growing body of literature is attempting to delimit the extent and nature of lower lithospheric structures in the Gulf Coast region and extend tectonic models to include this region (Dunn, 2008; Gao et al., 2008; Mosher et al., 2008; Poole et al., 2005). Here, we present new geochemical data on mantle xenoliths from Knippa, Texas, in order to better understand the relationship between the subcontinental lithospheric mantle and the overlying crustal basement of Laurentia along its southern structural edge. We integrate the geochemical data from the mantle xenoliths with geologic studies of the crustal basement, as well as geophysical studies of the deep crust and lithosphere, to generate possible scenarios for the origin of mantle metasomatism and discuss the implications of these scenarios for the evolution of the deep lithosphere beneath the Laurentian craton.

*Present address: Geology and Geophysics Department, Yale University, New Haven, Connecticut 06520-8109, USA.

GEOLOGIC SETTING

Lithospheric mantle xenoliths (spinel lherzolites) were collected from the Vulcan open-pit quarry in the town of Knippa at 29.29°N, 99.65°W, located in Uvalde County, Texas (Fig. 1). The xenoliths are hosted in a fine-grained, olivine nephenilite. There are also fine- to coarse-grained alkali basalts, olivine nephelinites, nepheline basanites, and phonolites in the area (Miggins et al., 2004). Series of Late Cretaceous basalts were erupted through Cretaceous shallow-marine sediments, forming mostly hypabyssal laccoliths, plugs, sills, and dikes, along with accumulations of ash and tuff that settled in water (Ewing and Caran, 1982). Miggins et al. (2004) dated the eruption of these basalts between 80 and 82 Ma based on $^{40}Ar/^{39}Ar$ chronology. The volcanoes have intruded through the buried Paleozoic structural belt (delimited by the trend of a potential field trough), where Mesozoic sediments overlie Proterozoic Laurentian basement (Flawn et al., 1961).

The Knippa basalts appear to be related to a much larger volcanic province that stretches from south-central Texas east through Oklahoma and Arkansas. Late Mesozoic alkali igneous activity occurs along the Ouachita belt in Texas, Arkansas, and Oklahoma (Byerly, 1991; see Fig. 1). Spencer (1969) recognized that these widely spaced volcanic centers were probably related temporally and tectonically, referring to the collection of volcanic centers as the "Balcones igneous province" because the trend of the volcanic rocks and hypabyssal intrusive laccoliths and plugs follows the buried Paleozoic Ouachita structural belt, which in Texas follows the Balcones escarpment. Magnetic surveys have since confirmed the extent of the Balcones igneous province (Ewing and Caran, 1982; Smith et al., 2001, 2008). In Figure 1, the locations of magmatic intrusions are reproduced from Ewing and Caran (1982). The locations of the Balcones and Luling faults are also shown. The broad zone of Cretaceous igneous activity in Texas is roughly bounded by the Balcones and Luling fault zones, and it lies inside the trend of a regional gravity anomaly. The exact origin of these basalts remains unclear and is a subject for further study. It has been suggested that sediment loading of the Gulf of Mexico could have concentrated flexure of the lithosphere near a structural hinge such as the Ouachita structural

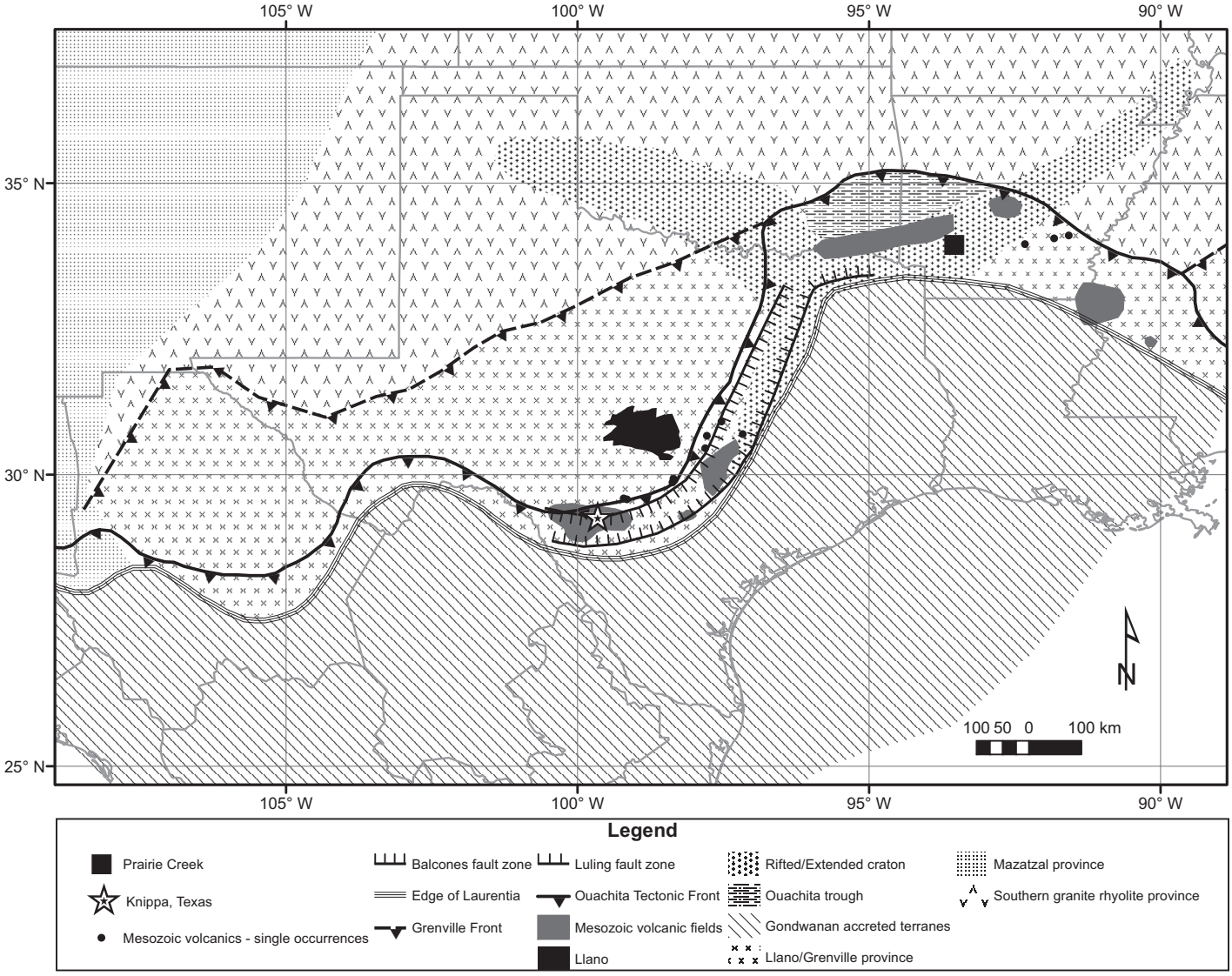

Figure 1. Location of Knippa samples and regional basement and structural features. Xenoliths from this study, and other Mesozoic volcanics, lie within the Balcones-Luling fault zone. Ouachita structures are represented as superimposed on Grenvillian lithosphere. The location of the Ouachita front is reproduced from Poole et al. (2005). The location of the edge of Laurentia is modified from Lambert et al. (1995) and Poole et al. (2005). Postulated rift segments from the breakup of Rodinia are modified from Dunn (2008), and the location of the Ouachita trough is from U.S. Geological Survey PACES gravity data. The Grenville front is reproduced generally from Hofman (1988).

belt (Miser, 1934), but flexure alone is not sufficient to cause melting because flexure (without erosion) does not lead to decompression of the mantle. Griffin et al. (2008) has suggested instead that the igneous province represents small-degree melts associated with decompressing asthenospheric mantle in response to lithospheric extension.

XENOLITH PETROGRAPHY

The xenoliths are clinopyroxene-poor lherzolites and harzburgites, containing variable proportions of olivine (ol), orthopyroxene (opx), clinopyoxene (cpx), and spinel (sp). The xenoliths occur as angular fragments within the basalt. Limited reaction between the host basalt and the xenoliths can be seen in the form of brownish, 1-mm-thick rims around the mantle xenoliths. The unreacted interiors of these xenoliths, however, still retain the original olivine-green color characteristic of unreacted peridotites.

Nine xenoliths were analyzed for this study. Modal abundances were difficult to calculate accurately because of the small size of the xenoliths (0.75–2 cm in diameter) and their coarse-grained nature (>1 mm). Modes were thus estimated by two methods. The first approach was point counting. However, many clinopyroxene (cpx) grains were much smaller than the average grain size of the xenoliths, and this resulted in either an overestimate or underestimate of cpx mode. To better assess cpx mode, we estimated the areal proportion of cpx in thin section (areal estimates and point counts of olivine [ol] and orthopyroxene [opx] modes were similar). The resulting mineral modes are 70–72% ol, 21–25% opx, 3–8% cpx, and ~2% spinel (sp) for samples 02A, 02F, 05A, 05B, 11B, and 15B. These modal mineralogies are similar to the dominant types of residual peridotite xenoliths worldwide. Two samples (01A and 08A) have

<3% cpx and are classified as refractory harzburgites. Sample 06E is anomalously low in opx (~10%), but, in every other respect, it is similar to the other lherzolites; this may be due to poor statistical sampling.

Texturally, the xenolith grains are coarse and equigranular to slightly tabular, and they have many well-developed triple junctions. Sample 08A is the only sample to show textural evidence for deformation: alignment of spinels and orthopyroxenes defines a weak foliation, and spinels occur as slightly elongated blebs. Clinopyroxenes of varying texture occur. Most cpx grains are heavily "corroded" with spongy or turbid textures, which we interpret to be due to flash-heating and decompression during ascent in the host basalt. Some clinopyroxenes have only a spongy rim, and this rim is diffuse when sharing an edge with orthopyroxene. Only the occasional large clinopyroxenes (~1.5 mm) have clear cores without any distinctive turbid textures. Orthopyroxenes have well-defined edges and occur in clusters. They are light green in plain light, and cleavage fractures are visible in plane polarized light. The olivine is equigranular to tabular shaped and coarse grained (up to 3 mm). The olivines are sometimes cut by thin serpentinized veins, which are associated with postemplacement weathering.

METHODS

Xenoliths were chosen for size and freshness, cut out of the host basalt, and made into 200-µm-thick, doubly polished sections for analytical work (as well as 30-µm-thick, doubly polished thin sections for petrographic analysis). Samples were analyzed for major and trace elements using laser ablation–inductively coupled plasma–mass spectrometry (LA-ICP-MS) using a ThermoFinnigan Element 2 ICP-MS at Rice University. Minerals in the thick sections were ablated using a 213 nm wavelength NewWave laser, pulsing at 10 Hz with a 55 µm spot size at 20 J/cm^2. Minerals analyzed were selected and targeted with the laser microscope viewfinder to avoid grain boundaries, inclusions, and cracks. We performed one medium- (major elements) and one low-mass-resolution (trace elements) analysis on the core of each mineral analyzed. For analyses, 10–12 cycles of background signal were recorded prior to firing the laser, and 30–40 cycles of signal were recorded during ablation. Drift effects and decay of the signal were corrected for using ^{25}Mg as an internal standard (Longerich et al., 1996). Three external basalt standards BHVO2 g, BIR1 g, and BCR2 g were simultaneously used for concentration calibrations. The ICP-MS and laser gases (helium) were tuned before analysis of standards and samples to attain a sensitivity of >600,000 cps for 15 ppm La in BHVO2 g (10 Hz, 55 µm spot size). Major-element concentrations were estimated from medium-resolution measurements by assuming all major and minor elements (Si, Mg, Ca, Fe, Mn, Ti, Na, K, Al) were oxides and that the oxides summed up to 100%. The resulting Mg content was then used as the internal standard for converting low-mass-resolution trace-element signals to concentrations.

Figure 2 is a typical example of the raw data. Signal intensities relative to Mg were constant during ablation for all elements except Rb, Cs, and Ba. Constant Mg-normalized signal intensities for a given element indicate homogeneity of that element on the time scales (and hence ablation depth) of ablation (~200 µm). Variable Mg-normalized signal intensities with time indicate heterogeneity. For example, in Figure 2A, the signal for Cs is orders of magnitude higher in the first half of ablation interval. Condie et al. (2004) have shown that large ion lithophile elements (LILEs) tend to accumulate along grain boundaries and in microcracks. We assume this to be the cause for variable intensities of Cs, Rb, and Ba, as opposed to surface contamination associated with sample preparation, because elevated Cs, Rb, and Ba signals also occur as pulses during ablation, not just at the start of ablation. These occasional pulses of Cs, Rb, and Ba are most evident in those cpx grains that have a "spongy" texture and thus may be related to microcracks or inclusions. No anomalous pulses were observed for Th, U,

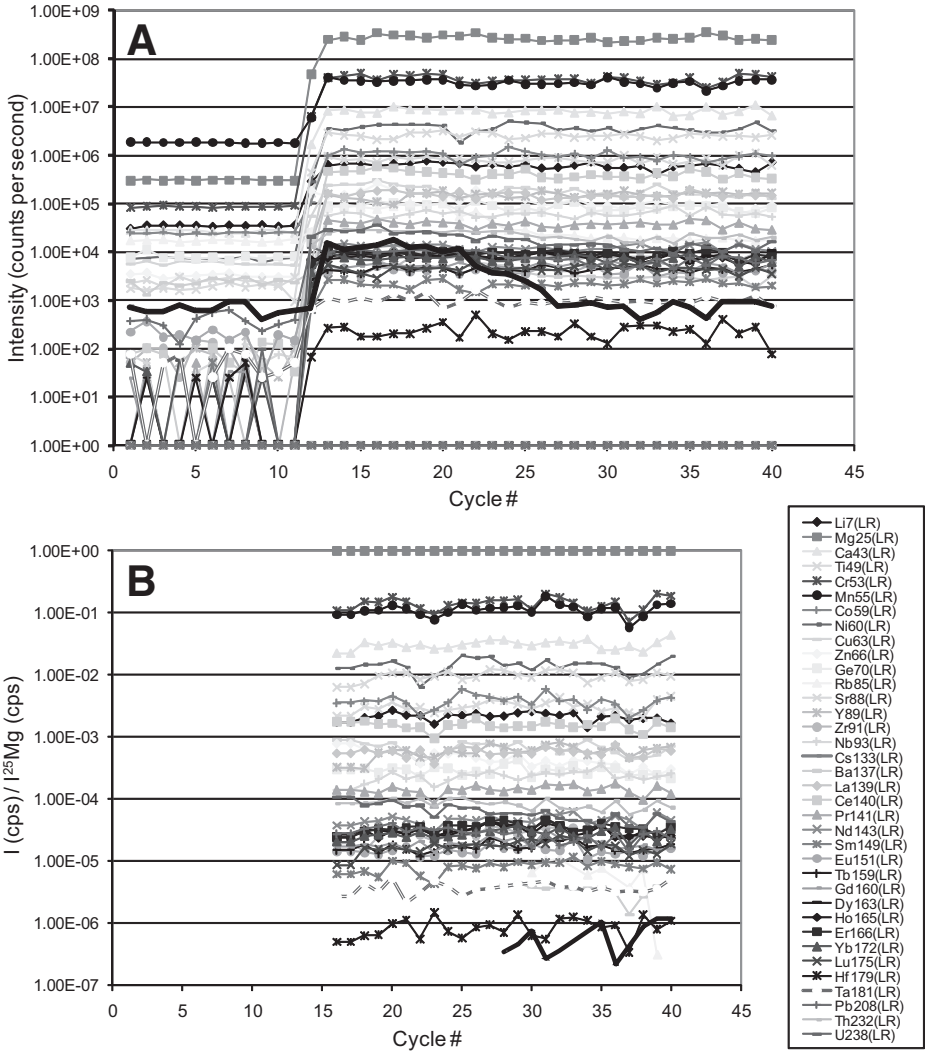

Figure 2. The raw data output of the inductively coupled plasma–mass spectrometry (ICP-MS) for one clinopyroxene from sample 05A. The first 10 counts are the background intensities. The analyzed data signal chosen from this shot is shown in B. Notice that Cs (bold, no marker) is variably enriched, but we eliminated that part of the signal that was not parallel to the other elements.

or Pb, which are often thought to behave similarly to Cs, Rb, and Ba.

Signal quality was ultimately assessed by examining time-resolved plots of normalized elemental intensities. Figure 2B shows that internally normalized ratios are constant and do not cross each other, indicating homogeneity for most elements. In the case of Cs, Rb, and Ba, their normalized intensities are not constant and therefore cross other normalized elements. We eliminated that part of the signal that was not parallel to the other elements. Nb and Zr in spinels suffered from CrAr isobaric interferences (Eggins et al., 1998) and were therefore discarded (in any case, Nb and Zr contents in peridotitic spinels are generally low and do not contribute a significant budget to the whole-rock Nb and Zr contents).

RESULTS

In Table 1, we present the modes, major oxide weight percents, and trace-element concentrations in ppm for mineral phases in each sample. These values reflect the average of all measurements run on the respective phase for that sample. In Table 2, we report the mineral modes, major oxide weight percents, trace-element concentrations in ppm, and calculated equilibration temperatures of the whole rock. Whole-rock compositions were estimated by summing up the mineral compositions according to their estimated proportions. In the case of 02F and 06E, spinels were too small to be analyzed, so the average composition of spinels in the other samples was used to reconstruct the major oxides for the bulk rock. We did not account for spinel in our trace-element reconstructions for the bulk rock because of its negligible effect on bulk-rock chemistry for all trace elements (except for Cr).

Thermobarometry

Temperatures of equilibration were estimated from Mg-Fe exchange between clinopyroxene and orthopyroxene using the method of Wells (1977) and Brey and Köhler (1990) after normalizing mineral major-element oxide compositions to 100 wt%. For the Brey and Köhler thermobarometer, a reasonable range of pressures for spinel lherzolites (2.0–2.5 GPa) was assumed. Our calculations indicate equilibration temperatures between 860 and 1142 °C using the Well's thermometer and between 820 and 1090 °C with the Brey and Köhler thermometer (one sample gave an anomalously low Brey and Köhler temperature of 786 °C) (Table 2). The average temperature of equilibration is 978 °C according to the method of Wells (1977) and 957 °C according to the method of Brey and Köhler (1990). A direct estimate of pressure was not possible because of the lack of appropriate mineral assemblages (e.g., garnet) for barometry.

Crude limits on pressure were determined by using the thermobarometric temperatures and fitting them to model continental geotherms (Fig. 3). The present-day surface heat flow in the region is ~50 mW/m^2 (Pollack et al., 1993; Woodruff and Foley, 1985), resulting in a depth of ~70 km for the minimum calculated temperature of 786 °C. However, given the large range in temperatures, these xenoliths could have equilibrated at pressures and depths approaching 3 GPa, but, due to the lack of garnet in these samples, they are unlikely to come from depths greater than ~85 km (Klemme, 2004). If heat flow was appreciably greater in the Cretaceous (70 mW/m^2), then the depth of equilibration could have been as shallow as 40 km, although this is unlikely given the passive nature of the margin at that time. We thus conclude that these xenoliths equilibrated at ~950 °C and at depths between 70 and 80 km. The pressure and temperature values of xenoliths appear to be associated with lithosphere that is thinner and warmer than typical Archean cratonic lithosphere, but significantly cooler than Phanerozoic lithospheric mantle, such as in the Basin and Range Province.

Major- and Minor-Element Chemistry

Mineral chemistries show similarities to continental lithospheric mantle samples. For example, Mg# ranges (molar Mg/[Mg + Fe]) of olivine, clinopyroxene, orthopyroxene, and whole rock are 0.89–0.91, 0.91–0.94, 0.89–0.91, and 0.89–0.91, respectively, and are slightly higher than that of primitive-mantle olivines (~0.89) but not as high as Archean cratonic mantle olivines (0.91–0.93). Al_2O_3 and Na_2O contents of pyroxenes are low, and the Ni contents of olivines are high, which are typical of continental peridotite xenoliths. These high Mg# values, high Ni contents, and low Al contents all suggest that these minerals are derived from refractory peridotites, such as harzburgites and clinopyroxene-poor lherzolites, though the possibility of some amount of refertilization cannot be excluded.

Whole-rock compositions, estimated by reconstructing mineral modes and compositions, are also consistent with a refractory origin. Compared to fertile lherzolite, such as model primitive-mantle compositions, the Knippa peridotites have high whole-rock MgO and low CaO, Na_2O, and Al_2O_3 values (Figs. 4A–4C). Error bars account for variations in estimated modal abundances, which far outweigh errors associated with mineral compositions. In a plot of CaO versus MgO (Fig. 4A), the Knippa peridotites fall within the same trend as seen in abyssal peridotites and peridotite xenoliths from Phanerozoic and Proterozoic continental lithosphere. There is no evidence from mineral modes or whole-rock chemistry to indicate that any of these samples are anomalously rich in Si, as is seen in some Archean cratonic mantle peridotites. The low Ca, Al, and Na contents and the negative correlation of these oxides with MgO are consistent with the Knippa peridotites representing the residues of previous melt depletion.

Trace-Element Chemistry

Primitive mantle–normalized (McDonough and Sun, 1995) trace-element spidergrams for reconstructed whole rocks are presented in Figure 5A and are plotted in order of increasing compatibility in the solid peridotite residue. Included compositions in these whole-rock reconstructions are the trace-element compositions of clinopyroxene, orthopyroxene, and olivine, but not spinel. The modal abundance of spinel is small, and the concentrations of trace elements in spinel are also small, so the effect of spinel on bulk trace-element compositions is negligible (Cr is an exception: spinel dominates the whole-rock Cr budget). In some cases, we were not able to measure the highly incompatible element abundances in olivine (e.g., light rare earth elements [LREEs]) because they were below detection limits, but the abundances of these elements are so low in olivine that they do not contribute to the bulk-rock composition. Thus, for the most part, the whole-rock trace-element budget is controlled by orthopyroxene and clinopyroxene.

A key feature of the whole-rock spidergrams is the depletion in moderately incompatible trace elements, such as the heavy rare earth elements (HREEs), relative to primitive mantle. In general, moderately incompatible elements, such as the HREEs, are more resistant to metasomatic disturbances (Canil, 2004; Lee et al., 2007a); hence, the HREE depletions likely reflect melt depletion. The HREE depletion also correlates with major-element indices of depletion, as can be seen by the correlation of Ca versus Lu (Fig. 4D).

Melt depletion, however, should result in positively sloping REE spidergrams (e.g., LREE depletion relative to HREEs) due to more efficient extraction of highly incompatible elements. However, "U-shaped" trends are seen, as exemplified by the relative enrichment in LREEs. High La/Sm and Sm/Yb ratios in our samples are reminiscent of metasomatized

TABLE 1. MINERAL MODES AND COMPOSITIONS

Sample	01A				02A				02F			
	ol	opx	cpx	sp	ol	opx	cpx	sp	ol	opx	cpx	sp
Modes:	0.72	0.25	0.01	0.02	0.72	0.23	0.03	0.02	0.71	0.225	0.045	0.02
(wt%)												
SiO_2	37.9	57.2	50.2	0.141	38.1	56.1	49.4	0.0497	40.3	57.2	52.2	N/A
TiO_2	0.00796	0.0636	0.314	0.117	0.00465	0.117	0.487	0.440	0.00190	0.0397	0.179	N/A
Al_2O_3	0.818	2.60	3.14	48.1	0.0235	2.22	3.80	37.2	0.0347	3.30	3.87	N/A
Cr_2O_3	0.107	0.376	0.798	20.0	0.0105	0.363	1.14	24.6	0.0109	0.370	0.754	N/A
FeO	9.29	6.01	2.41	13.2	9.22	6.90	3.28	16.7	9.49	6.36	2.88	N/A
MnO	0.160	0.153	0.0867	0.146	0.130	0.167	0.0879	0.153	0.134	0.149	0.102	N/A
MgO	51.5	32.7	18.3	19.1	51.5	33.2	18.3	18.0	52.0	34.7	18.9	N/A
CaO	0.128	0.435	23.4	0.00	0.0378	0.393	21.5	0.00993	0.0562	0.562	21.7	N/A
Na_2O	0.0319	0.0399	0.896	0.00	0.0324	0.0551	1.44	0.00780	0.00657	0.0929	1.57	N/A
K_2O	0.00962	0.0123	0.00296	0.00	0.00873	0.0000469	0.0271	0.0181	0.00	0.00	0.0129	N/A
Sum	99.9	99.6	99.5	101	99.0	99.8	99.4	97.2	102	99.8	102	N/A
Mg#	90.6				90.4				90.5			
Trace concentration (ppm)												
Li	1.62	1.75	26.3	0.189	2.02	2.06	34.7	6.25	3.20	57.6	25.9	N/A
Ti	7.28	219	695	447	20.6	788	3190	59.1	5.23	304	1210	N/A
Cr	57.6	3140	5980	112000	49.7	2670	8320	4210	50.5	4050	11800	N/A
Mn	1070	1030	593	788	1090	1220	580	436	789	1970	1210	N/A
Co	155	58.3	22.4	185	138	67.4	20.3	70.3	112	110	40.2	N/A
Ni	3360	780	348	1730	3220	809	284	1270	2410	1340	597	N/A
Cu	0.985	0.259	3.19	N/A	N/A	0.00647	2.47	0.306	N/A	N/A	N/A	N/A
Zn	57.8	37.7	11.2	N/A	N/A	39.9	12.8	59.4	N/A	N/A	N/A	N/A
Y	0.00969	0.387	6.03	0.0102	0.0167	0.763	16.3	0.00925	0.0236	1.12	30.2	N/A
Cs	0.000965	0.000999	0.00322	0.0206	0.00191	0.00185	0.00730	0.0142	0.000155	BDL	0.606	N/A
Rb	0.00523	0.0466	0.155	0.486	0.100	0.0220	0.351	0.355	0.0154	0.141	6.89	N/A
Ba	0.0722	0.0137	0.227	0.138	0.305	BDL	1.54	0.647	0.0462	0.372	24.0	N/A
Nb	0.00240	0.0395	0.267	N/A	BDL	0.0325	0.225	N/A	0.00123	0.0822	1.31	N/A
Ta	0.00220	0.00154	0.0244	0.0000512	0.00241	0.000402	0.0157	0.000409	BDL	0.00467	0.120	N/A
La	0.000238	0.00199	1.15	0.00294	0.00192	0.0150	14.4	0.00267	0.00155	0.0192	28.8	N/A
Ce	0.00283	0.00728	3.13	0.00968	0.00743	0.0372	28.9	0.00607	0.00382	0.0853	83.7	N/A
Pr	0.000941	0.00156	0.431	0.00183	0.000720	0.00519	2.79	0.000562	0.000398	0.00801	10.4	N/A
Sr	0.00852	0.0325	21.4	0.128	0.0193	0.292	363	0.962	0.0445	0.227	478	N/A
Nd	0.00244	0.0102	2.25	0.00229	BDL	0.0352	10.6	0.00443	0.00243	0.0395	42.8	N/A
Sm	0.00374	0.0110	0.806	0.00945	BDL	0.0149	2.39	0.000262	BDL	0.0344	8.81	N/A
Zr	0.0271	0.610	9.79	N/A	0.112	1.34	47.4	N/A	0.0708	0.653	130	N/A
Hf	0.0119	0.0291	0.469	0.00280	0.00849	0.0114	0.944	0.00146	BDL	0.00897	1.27	N/A
Eu	0.000153	0.00425	0.282	BDL	0.000148	BDL	0.851	BDL	BDL	0.0152	2.78	N/A
Gd	0.00510	0.0223	1.10	0.00392	0.00426	0.0483	2.76	BDL	BDL	0.0495	7.17	N/A
Tb	0.000763	0.00482	0.172	0.000537	BDL	0.00816	0.427	BDL	0.000869	0.0122	1.02	N/A
Dy	0.00222	0.0503	1.15	0.00481	0.00503	0.0881	2.94	BDL	0.00333	0.134	5.91	N/A
Ho	0.000752	0.0138	0.232	BDL	0.00130	0.0207	0.592	0.000370	0.000783	0.0396	1.09	N/A
Er	0.00385	0.0536	0.613	BDL	BDL	0.0975	1.62	BDL	0.00552	0.167	2.96	N/A
Yb	0.00765	0.0936	0.520	0.00370	0.0131	0.153	1.44	0.00337	0.0128	0.266	2.82	N/A
Lu	0.00345	0.0185	0.0773	0.000577	0.00297	0.0280	0.214	0.00155	0.00364	0.0561	0.427	N/A
Pb	0.00200	0.00602	0.0645	0.421	0.0228	0.00365	1.19	0.0295	0.00772	0.0294	0.497	N/A
Th	0.000638	0.000758	0.0447	BDL	BDL	0.00296	0.334	BDL	0.00139	0.0112	1.20	N/A
U	BDL	0.000724	0.0267	0.00145	0.00163	0.00189	0.0956	0.000352	0.000573	0.0133	0.331	N/A

(continued)

TABLE 1. MINERAL MODES AND COMPOSITIONS *(continued)*

Sample	05A				05B				06E			
	ol	opx	cpx	sp	ol	opx	cpx	sp	ol	opx	cpx	sp
Modes:	0.7	0.21	0.07	0.02	0.7	0.225	0.065	0.02	0.7	0.235	0.045	0.02
(wt%)												
SiO_2	40.0	60.1	56.0	0.162	42.4	62.5	57.1	0.126	40.0	58.7	56.4	N/A
TiO_2	0.000900	0.0281	0.132	0.0583	0.00089	0.0300	0.147	0.0508	0.00182	0.0367	0.266	N/A
Al_2O_3	0.0109	2.74	3.20	47.7	0.0115	3.03	2.85	50.1	0.0244	2.48	2.92	N/A
Cr_2O_3	0.00973	0.382	0.808	17.5	0.00632	0.269	0.606	12.8	0.0103	0.359	0.703	N/A
FeO	9.53	5.83	2.23	11.3	10.6	6.19	2.41	12.3	10.4	5.89	2.60	N/A
MnO	0.161	0.154	0.0868	0.137	0.192	0.173	0.0887	0.131	0.164	0.141	0.0447	N/A
MgO	51.3	31.7	16.7	22.8	48.0	29.0	16.7	24.2	50.5	32.0	18.1	N/A
CaO	0.0418	0.487	21.5	0.00460	0.0313	0.397	20.7	0.0118	0.0426	0.369	21.3	N/A
Na_2O	0.00161	0.0637	1.02	0.00	0.00551	0.0700	0.895	0.00	0.00418	0.0394	0.982	N/A
K_2O	0.00	0.00107	0.00369	0.0106	0.00	0.00731	0.0607	0.00694	0.00	0.0220	0.180	N/A
Sum	101	99.8	102	99.8	101	99.8	102	99.7	101	99.8	104	N/A
Mg#	90.5				89.0				89.6			
Trace concentration (ppm)												
Li	2.37	3.02	19.0	0.436	1.48	2.75	8.71	0.412	4.44	1.51	2.81	N/A
Ti	4.81	140	406	315	4.22	141	524	290	7.68	0.0133	1070	N/A
Cr	72.9	3020	6480	121000	52.3	2350	5070	98400	67.2	0.0378	6940	N/A
Mn	1220	1100	614	913	1390	1110	609	1010	1180	0.392	598	N/A
Co	173	62.4	20.4	273	178	57.5	17.8	272	176	0.526	24.3	N/A
Ni	3190	846	298	2650	3520	708	206	3220	3290	0.583	360	N/A
Cu	1.17	0.919	3.54	5.29	0.157	0.265	0.518	2.25	0.929	0.0165	1.23	N/A
Zn	54.1	34.4	10.1	914	70.2	38.7	12.1	1430	58.0	0.379	11.0	N/A
Y	0.0120	0.335	5.51	0.00746	0.0135	0.395	8.34	0.0104	0.0201	0.0237	10.4	N/A
Cs	0.000260	0.00116	0.0109	0.00162	0.0000867	0.00664	0.241	0.0122	BDL	2.94	0.103	N/A
Rb	0.00263	0.0149	0.234	0.0655	BDL	0.107	4.85	0.148	BDL	2.63	2.87	N/A
Ba	0.0525	0.0674	8.03	0.0492	BDL	0.274	11.0	0.369	BDL	0.0679	20.1	N/A
Nb	0.00653	0.0713	1.16	N/A	BDL	0.0326	0.130	N/A	0.00461	0.0537	0.913	N/A
Ta	0.000736	0.00112	0.0309	0.00209	BDL	BDL	0.00506	0.000101	0.000859	0.0105	0.0319	N/A
La	0.00146	0.0161	7.75	0.000890	BDL	0.00446	4.44	0.00457	0.000645	0.168	15.8	N/A
Ce	0.00165	0.0467	15.5	0.00546	0.00101	0.0171	12.5	0.0129	0.00373	0.246	39.8	N/A
Pr	0.000787	0.00526	1.20	BDL	BDL	0.00240	1.14	BDL	0.00185	0.133	3.95	N/A
Sr	0.0207	0.159	88.1	0.0473	BDL	0.154	70.5	0.281	0.00177	0.206	327	N/A
Nd	0.00485	0.0247	3.44	0.00546	0.00400	0.00940	3.48	0.00811	BDL	0.0867	13.5	N/A
Sm	0.00339	0.00761	0.516	0.00353	BDL	0.00605	0.558	BDL	BDL	0.0386	2.29	N/A
Zr	0.00835	0.319	3.58	N/A	BDL	0.140	0.630	N/A	0.0174	0.0144	10.9	N/A
Hf	0.00212	0.00785	0.0667	BDL	0.00440	0.00333	0.0535	BDL	0.00417	0.0304	0.331	N/A
Eu	0.00277	0.00238	0.195	0.00458	0.0000143	0.00247	0.251	0.00947	BDL	BDL	0.824	N/A
Gd	0.00184	0.0162	0.583	0.00245	0.00220	0.0126	0.805	0.00318	0.00100	0.0253	1.98	N/A
Tb	BDL	0.00354	0.104	BDL	0.000748	0.00345	0.158	0.000753	BDL	0.0316	0.293	N/A
Dy	0.00192	0.0361	0.833	0.000918	0.00137	0.0377	1.33	0.00579	0.00261	0.0231	1.84	N/A
Ho	0.000676	0.0120	0.202	0.000231	0.000659	0.0140	0.316	0.000350	BDL	0.0222	0.394	N/A
Er	0.00265	0.0515	0.641	BDL	0.00260	0.0623	0.953	BDL	0.00761	0.0195	1.10	N/A
Yb	0.00916	0.101	0.711	BDL	BDL	0.116	0.985	0.00363	0.0169	0.0282	1.11	N/A
Lu	0.00290	0.0220	0.117	BDL	0.00330	0.0284	0.164	BDL	0.00616	0.0514	0.175	N/A
Pb	0.00749	0.00582	0.275	0.00578	0.00479	0.00492	0.0886	0.0107	0.00247	0.625	0.392	N/A
Th	0.00222	0.0113	1.17	0.00151	0.000508	0.00168	0.170	0.000596	BDL	0.0750	1.20	N/A
U	0.000698	0.00855	0.384	0.000603	0.000165	0.000932	0.0655	0.00125	0.000100	0.126	0.320	N/A

(continued)

TABLE 1. MINERAL MODES AND COMPOSITIONS *(continued)*

Sample	08A				11B				15B			
	ol	opx	cpx	sp	ol	opx	cpx	sp	ol	opx	cpx	sp
Modes:	0.71	0.24	0.03	0.02	0.71	0.22	0.05	0.02	0.7	0.23	0.05	0.02
(wt%)												
SiO_2	40.2	58.4	51.0	0.105	38.3	53.8	50.5	0.290	40.9	56.0	50.6	0.656
TiO_2	0.00114	0.0329	0.214	0.0551	0.000800	0.0296	0.131	0.103	0.00164	0.0573	0.257	0.0942
Al_2O_3	0.00705	3.16	3.19	46.8	0.00400	2.74	2.65	39.0	0.0116	3.40	3.21	46.9
Cr_2O_3	0.00919	0.372	1.08	17.2	0.00856	0.565	0.928	23.2	0.0100	0.388	0.716	18.5
FeO	10.6	6.38	2.60	11.8	10.4	7.72	2.38	13.5	9.47	5.89	2.40	11.7
MnO	0.173	0.151	0.0970	0.120	0.139	0.169	0.0715	0.126	0.136	0.140	0.0843	0.112
MgO	52.2	33.0	20.4	21.1	52.4	35.5	17.8	21.0	49.3	33.1	19.7	19.8
CaO	0.0397	0.484	22.0	0.00869	0.0265	0.419	21.3	0.0190	0.0332	0.464	21.7	0.00
Na_2O	0.00130	0.0659	0.629	0.00555	0.00322	0.0500	0.970	0.00	0.00527	0.0545	0.745	0.00474
K_2O	0.00	0.00	0.0622	0.0101	0.00	0.0122	0.0310	0.00500	0.00	0.000165	0.0160	0.000195
Sum	103	99.8	101	97.3	101	99.8	96.7	97.3	99.9	99.8	99.5	97.8
Mg#	89.8				90.3				90.3			
Trace concentration (ppm)												
Li	3.38	2.37	25.6	2.18	2.21	2.12	28.2	0.769	5.47	4.30	1.46	0.00
Ti	5.08	130	526	347	4.84	160	345	703	8.04	302	1930	510
Cr	68.9	3330	6570	112000	66.9	3380	5830	157000	44.8	2520	7890	123000
Mn	1290	1130	662	805	1110	1160	490	989	943	955	785	724
Co	188	57.5	29.3	227	158	65.7	19.8	250	121	49.8	38.3	191
Ni	3990	901	425	2120	3200	834	286	1550	2970	665	682	2050
Cu	BDL	BDL	BDL	5.58	0.518	0.328	3.10	3.60	N/A	N/A	N/A	N/A
Zn	BDL	BDL	BDL	789	56.7	38.0	9.15	976	N/A	N/A	N/A	N/A
Y	0.0255	0.600	12.5	0.0199	0.0127	0.522	6.69	0.0216	0.0121	0.402	12.0	0.00188
Cs	0.000542	0.000747	0.00733	0.0504	BDL	0.00183	0.000393	BDL	0.00203	0.00	0.109	0.00165
Rb	0.0277	0.0689	0.0999	1.23	BDL	0.0135	0.0443	0.0700	0.0400	0.0128	1.72	0.0226
Ba	0.112	0.202	1.26	2.12	0.0111	0.00	0.223	0.237	0.0155	0.000405	0.854	BDL
Nb	0.0156	0.338	2.35	N/A	0.00466	0.0556	0.310	N/A	0.00241	0.0104	0.875	N/A
Ta	0.0000107	0.00177	0.295	0.00610	BDL	0.00153	0.0207	0.00293	0.00196	0.00	0.0482	0.00256
La	BDL	0.0107	8.34	0.00988	BDL	0.0124	7.96	0.00676	0.000550	0.00413	9.68	BDL
Ce	0.0111	0.0351	19.4	0.0194	0.00293	0.0505	20.3	0.0226	0.00178	0.00852	13.9	0.00296
Pr	0.00196	0.00401	2.20	0.00155	0.000883	0.00777	2.11	0.00222	0.00	0.00143	1.11	0.00113
Sr	0.00908	0.104	109	1.23	0.00260	0.234	149	0.595	0.0301	0.105	205	0.0417
Nd	0.00212	0.0320	8.81	0.00269	BDL	0.0452	7.58	0.0151	0.00	0.00646	4.04	0.00451
Sm	0.00470	0.0160	1.82	0.00436	0.00364	0.0242	1.30	0.00991	0.0144	0.0114	1.23	0.0129
Zr	0.160	3.58	69.3	N/A	0.0131	0.828	11.1	N/A	0.0120	0.291	14.2	N/A
Hf	0.00575	0.0296	0.608	0.00594	BDL	0.0172	0.231	0.00235	0.00147	0.0176	0.515	BDL
Eu	0.00129	0.00538	0.426	0.000474	0.00284	0.00710	0.422	BDL	0.000406	0.00202	0.546	0.00175
Gd	BDL	0.0190	1.81	BDL	0.00701	0.0360	1.33	BDL	0.00230	0.0210	1.82	BDL
Tb	0.000442	0.00376	0.260	0.000778	BDL	0.00918	0.198	BDL	0.000289	0.00360	0.321	BDL
Dy	0.00349	0.0475	1.96	0.00293	BDL	0.0724	1.25	BDL	0.00196	0.0447	2.10	0.00481
Ho	0.00160	0.0217	0.484	0.000399	BDL	0.0222	0.259	BDL	0.000740	0.0150	0.472	0.000909
Er	0.00626	0.0902	1.36	0.00154	0.00407	0.0847	0.693	BDL	0.00356	0.0640	1.29	BDL
Yb	0.0133	0.148	1.19	BDL	0.0127	0.150	0.609	BDL	0.0100	0.113	1.25	BDL
Lu	0.00363	0.0304	0.182	0.000709	0.00312	0.0279	0.0911	0.000266	0.00334	0.0221	0.169	0.00343
Pb	0.00685	0.0186	0.412	0.0106	0.0133	0.00570	0.795	0.0375	0.00541	0.00331	0.461	0.00644
Th	0.00151	0.00426	0.628	0.00997	0.00236	0.00496	0.326	0.00191	0.000533	BDL	0.139	0.000494
U	0.000546	0.00401	0.232	0.00600	0.00144	0.00489	0.0999	0.00210	0.000293	0.00102	0.0843	BDL

Note: BDL—below detection limit; ol—olivine; cpx—clinopyroxene; opx—orthopyroxene; sp—spinel.

TABLE 2. BULK COMPOSITION

	Sample								
	01A	02A	02F	05A	05B	06E	08A	11B	15B
Modes									
Ol	0.72	0.72	0.71	0.7	0.7	0.7	0.71	0.71	0.7
opx	0.25	0.23	0.225	0.21	0.225	0.235	0.24	0.22	0.23
cpx	0.01	0.03	0.045	0.07	0.065	0.045	0.03	0.05	0.05
sp	0.02	0.02	0.02	0.02	0.02	0.02	0.02	0.02	0.02
(wt%)									
SiO_2	42.1	41.8	43.8	44.6	47.4	44.3	44.1	41.6	44.1
TiO_2	0.0271	0.0536	0.0271	0.0170	0.0179	0.0307	0.0162	0.0157	0.0291
Al_2O_3	2.23	1.39	1.69	1.76	1.88	1.48	1.80	1.52	1.89
Cr_2O_3	0.579	0.618	0.617	0.494	0.360	0.615	0.473	0.641	0.501
FeO	8.48	8.66	8.64	8.28	9.20	9.15	9.36	9.48	8.34
MnO	0.158	0.138	0.137	0.154	0.181	0.153	0.164	0.142	0.134
MgO	45.8	45.6	45.9	44.2	41.7	44.0	46.0	46.3	43.5
CaO	0.434	0.762	1.14	1.63	1.46	1.07	0.805	1.18	1.22
Na_2O	0.0419	0.0793	0.0966	0.0862	0.0778	0.0565	0.0357	0.0618	0.0536
K_2O	0.0100	0.00747	0.000942	0.000696	0.00607	0.0144	0.00357	0.00433	0.00355
Sum	99.8	99.1	102	101	102	101	103	101	99.7
Mg# in ol.	90.6	90.4	90.5	90.5	89.0	89.6	89.8	90.3	90.3
Eq. temp. °C (Wells, 1977)	873	891	893	1034	1142	1066	1040	864	1007
TBKN (1.5–2.0 GPa)	782–789	862–870	848–856	1019–1028	1088–1078	1066–1078	977–986	820–827	955–963
Trace concentration (ppm)									
Li	1.87	3.10	16.4	3.63	2.23	3.59	3.78	3.46	4.89
Ti	76.0	293	126	67.4	74.6	53.6	57.6	70.0	182
Cr	3130	983	1480	3570	2860	360	3290	4220	3470
Mn	1050	1090	1060	1140	1280	852	1220	1080	934
Co	130	117	106	141	144	124	153	133	102
Ni	2650	2540	2040	2490	2700	2320	3110	2500	2300
Cu	0.806	0.0816	N/A	1.37	0.248	0.710	N/A	N/A	N/A
Zn	51.1	10.8	N/A	64.1	87.1	41.2	N/A	N/A	N/A
Y	0.164	0.677	1.63	0.465	0.641	0.489	0.539	0.459	0.702
Cs	0.00139	0.00231	0.0274	0.00122	0.0175	0.696	0.00179	0.000422	0.00691
Rb	0.0267	0.0949	0.353	0.0227	0.342	0.748	0.0639	0.00659	0.117
Ba	0.0605	0.279	1.20	0.614	0.782	0.922	0.208	0.0238	0.0536
Nb	0.0143	0.0142	0.0781	0.101	0.0158	0.0569	0.163	0.0311	0.0478
Ta	0.00221	0.00231	0.00646	0.00296	0.000331	0.00452	0.00942	0.00143	0.00384
La	0.0122	0.437	1.30	0.547	0.289	0.749	0.253	0.401	0.485
Ce	0.0353	0.881	3.79	1.09	0.815	1.85	0.598	1.03	0.700
Pr	0.00541	0.0855	0.469	0.0854	0.0744	0.211	0.0684	0.108	0.0558
Sr	0.230	11.0	21.6	6.22	4.62	14.8	3.32	7.53	10.3
Nd	0.0268	0.327	1.93	0.249	0.231	0.628	0.274	0.389	0.204
Sm	0.0137	0.0750	0.404	0.0402	0.0376	0.112	0.0619	0.0732	0.0745
Zr	0.270	1.81	6.04	0.323	0.0724	0.508	3.05	0.747	0.788
Hf	0.0206	0.0371	0.0592	0.00780	0.00731	0.0250	0.0295	0.0154	0.0308
Eu	0.00399	0.0257	0.129	0.0162	0.0171	0.0371	0.0150	0.0247	0.0281
Gd	0.0203	0.0969	0.334	0.0456	0.0568	0.0959	0.0588	0.0796	0.0975
Tb	0.00348	0.0147	0.0494	0.00799	0.0116	0.0206	0.00903	0.0119	0.0171
Dy	0.0258	0.112	0.298	0.0673	0.0961	0.0902	0.0728	0.0783	0.117
Ho	0.00631	0.0235	0.0587	0.0171	0.0242	0.0229	0.0209	0.0178	0.0276
Er	0.0223	0.0711	0.174	0.0575	0.0778	0.0595	0.0669	0.0562	0.0818
Yb	0.0342	0.0879	0.196	0.0774	0.0902	0.0686	0.0807	0.0725	0.0953
Lu	0.00789	0.0150	0.0344	0.0148	0.0194	0.0243	0.0154	0.0129	0.0159
Pb	0.0120	0.0536	0.0345	0.0258	0.0104	0.166	0.0219	0.0512	0.0277
Th	0.00110	0.0107	0.0575	0.0857	0.0118	0.0716	0.0211	0.0191	0.00735
U	0.000477	0.00449	0.0183	0.0292	0.00461	0.0441	0.00844	0.00713	0.00466

Note: TBKN—method of Brey and Köhler (1990).

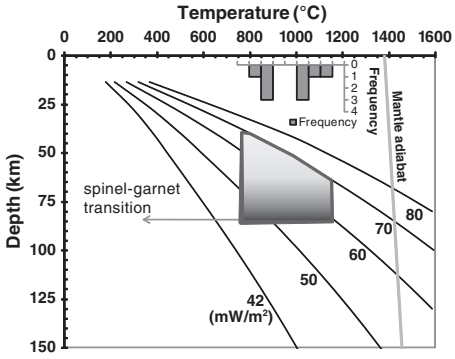

Figure 3. Using models of Pollack et al. (1993), we calculate the pressure and temperature (*P-T*) profile for continents under various surface heat-flow conditions. The range of *P-T* conditions for the Knippa samples is constrained by their calculated temperatures of equilibration, the 85 km spinel-garnet transition, and reasonable geotherms (modern-day surface heat flux of ~50 mW/m² is consistent with a cool, thick lithosphere).

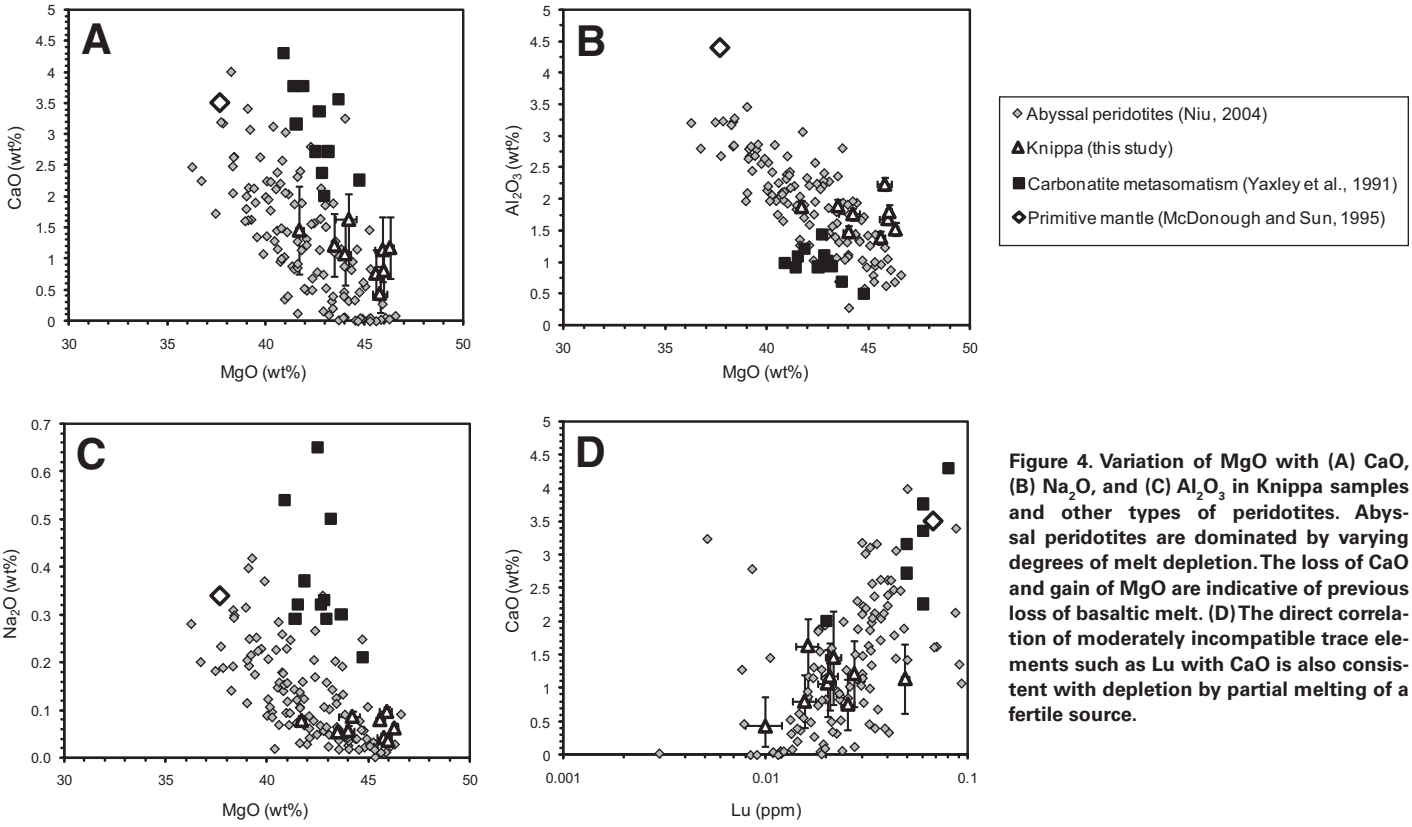

Figure 4. Variation of MgO with (A) CaO, (B) Na_2O, and (C) Al_2O_3 in Knippa samples and other types of peridotites. Abyssal peridotites are dominated by varying degrees of melt depletion. The loss of CaO and gain of MgO are indicative of previous loss of basaltic melt. (D) The direct correlation of moderately incompatible trace elements such as Lu with CaO is also consistent with depletion by partial melting of a fertile source.

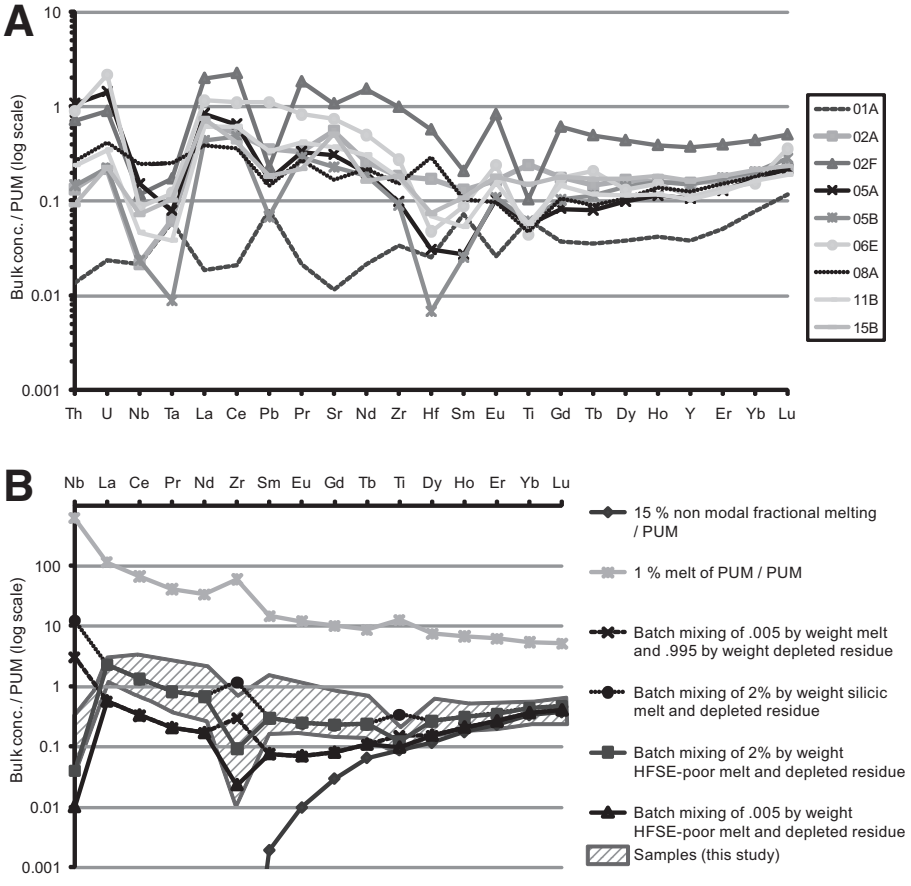

Figure 5. (A) The bulk concentration of trace elements in each sample of this study, normalized to primitive mantle. Elements are ordered to reflect thermodynamic similarity under anhydrous conditions. Most samples from the Knippa locality are preferentially enriched in light rare earth elements (LREEs) over Nb, Ta, and Pb, as well as being preferentially enriched in middle (M) REEs over Zr, Hf, and Ti. Samples 01A and 08A do not fit the general pattern, although these samples have the most refractory mineral modes. (B) Theoretically calculated, primitive mantle–normalized concentration of elements in a depleted, unserpentinized mantle residue, and concentrations of elements in an anhydrous 1% melt of fertile mantle. Samples from this study are in the field with the diagonal shading. The two curves that pass through the sample field are the result of mixing the depleted residue with the basaltic melt (enriched in high field strength elements [HFSE]) or a HFSE-depleted melt/fluid.

mantle xenoliths in subarc or post-Archean continental settings, as well as enriched magmas such as arc magmas (Fig. 6). They do not match the highly LREE-depleted signatures of oceanic abyssal peridotites (Niu, 2004), nor do they match typical mid-ocean-ridge basalts (MORBs), which are also depleted in LREEs relative to HREEs. Carbonatite-metasomatized xenoliths (Yaxley et al., 1991) have much steeper LREE enrichment patterns than the Knippa peridotites. These observations suggest that these xenoliths were cryptically reenriched in incompatible trace elements after the melt depletion event that gave rise to their refractory major-element compositions.

We also examined the high field strength element (HFSE) abundances: Nb, Ta, Zr, Hf, and Ti. It is generally thought that depletion in these elements relative to the REE partner that exhibits the most similar bulk partition coefficients during anhydrous peridotite melting is a sign of hydrous fluid metasomatism because the HFSEs are considered to be much less fluid mobile than the REEs. Relative depletions in these elements occur in our clinopyroxene grains, but these relative depletions in clinopyroxene do not by themselves imply metasomatism by HFSE-depleted fluids/melts, since such depletions commonly occur in clinopyroxene grains from other mantle xenolith suites (much of the whole-rock HFSE budget is also housed in orthopyroxene). Thus, whole rocks often show little HFSE depletion even though clinopyroxenes are HFSE depleted. However, this is not the case in the Knippa samples. In all but two of the most refractory samples (01A and 08A), the reconstructed whole-rock HFSEs show relative depletions. For example, whole-rock Nb and Ta are depleted relative to La; Zr and Hf are depleted relative to Sm; and Ti is depleted relative to Eu. These HFSE depletions are typically found only in arc magmas or in mantle xenoliths that have been metasomatized by fluids (Kelemen et al., 1993). Because of the low fluid solubilities of HFSEs compared to REEs, fluid metasomatism typically yields HFSE-depletion signatures, whereas no HFSE anomalies are generated during silicate melt metasomatism.

Large ion lithophile elements (LILEs), such as Ba, Cs, and Rb, were more difficult to reconstruct because of their low concentrations in silicate minerals. We observed enrichments in these elements in some clinopyroxenes. Figure 7 shows the primitive mantle–normalized concentrations of trace elements in clinopyroxenes from sample 05A. As discussed in the petrography section, two textures of clinopyroxenes exist, the more common being the "turbid" clinopyroxene. Turbid clinopyroxenes show variable but high concentrations of Cs, Rb, and Ba. The clear-cored clinopyroxenes of 05A (two shots, a and b) have much lower concentrations of LILEs. In addition, we also found that the rims of clinopyroxenes showed enrichment in these elements compared to the core; thus, it is not clear what fraction of these enrichments is due to ancient fluid-metasomatic events or more recent disturbances associated with the magmatic precursor to the host magma.

Assessing Trace-Element Equilibrium

An important question regarding trace-element compositions of mantle xenoliths is whether the compositions are actually representative of the mantle or if they represent recent perturbations associated with contamination by the host magma. One way to address this problem is to assess whether the mineral chemistries have equilibrated. If the mineral chemistries have been recently disturbed, they should be out of equilibrium. Using extension of lattice strain theory to mineral-mineral element partitioning, Lee et al. (2007a) and Agranier and Lee (2007) showed that when equilibrium exists between mantle pyroxenes, there is a nearly log-linear variation in the ratio C(opx)/C(cpx) with increasing ionic radius of the lanthanide series. Samples that have been contaminated or recently metasomatized show deviations from this log-linear trend. Figure 8 demonstrates that there is, for the most part, a log-linear variation in the concentrations of REEs in orthopyroxene over clinopyroxene for the Knippa peridotites. These observations indicate that, at least for the REEs, equilibrium has been achieved, and the reconstructed whole-rock REE patterns are probably representative of the mantle. While we have not been able to do the same for the HFSEs, we assume that the high degree of equilibrium seen in the REEs hints that the HFSEs are also in equilibrium.

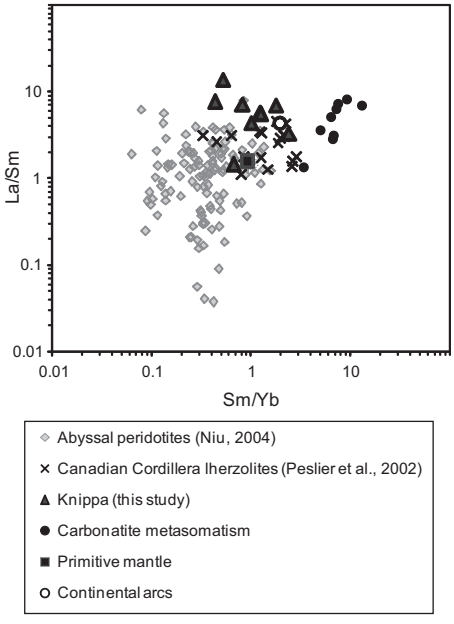

Figure 6. The bulk concentration of La/Sm versus Sm/Yb for the Knippa samples, primitive upper mantle (McDonough and Sun, 1995), continental arc material, Cascadian xenoliths, SE Australian carbonatite-influenced xenoliths (Yaxley et al., 1991), and global oceanic peridotites (Niu, 2004). The Knippa and continental materials all have La/Sm ratios above primitive mantle, while oceanic materials have La/Sm and Sm/Yb ratios lower than primitive mantle. Only the Yaxley samples have significant middle rare earth element (MREE) enrichment.

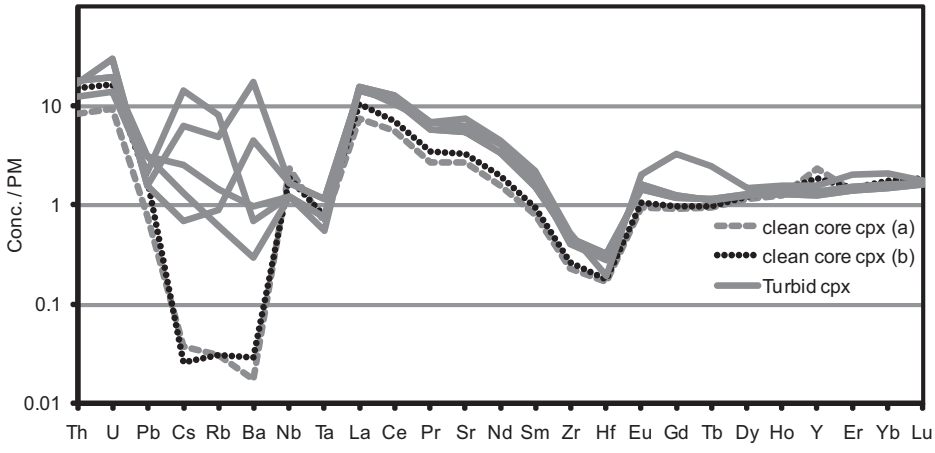

Figure 7. Multi-element, primitive mantle (PM)–normalized spidergram for several clinopyroxene (cpx) grains from the same xenolith (05A). Notice the variability in concentration of Cs, Rb, and Ba between different textures and between grains of turbid texture. For this reason, bulk abundances of these elements are very uncertain.

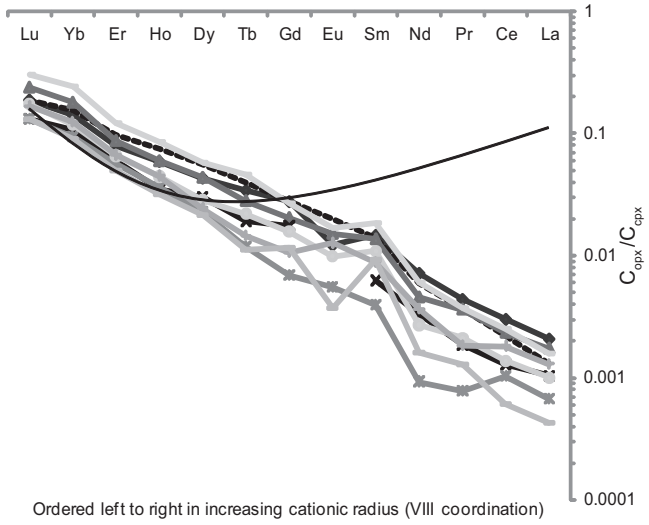

Figure 8. The ratio of the concentration of rare earth elements (REEs) in orthopyroxene over clinopyroxene versus decreasing cationic lattice radius in the cores of minerals from sample 05A of this study. The trend is typical of all samples in the study, including the negative divergence from theory at Eu. The data are plotted with the theoretical partition coefficients calculated from lattice strain theory by Lee et al. (2007a). When equilibrium is achieved, the partition coefficients (Dopx/cpx) ~ K (the equilibrium constant) ~ (Copx/Ccpx). The plot shows that the samples analyzed are in fact in thermodynamic equilibrium for rare earth elements.

DISCUSSION

Geochemical Signature of Subduction

The Knippa xenoliths have whole-rock and mineral chemistries characteristic of the subcontinental lithospheric mantle. Equilibration temperatures of 800–1100 °C are too cool to be associated with hot plumes or asthenospheric mantle. Interpolating from model geotherms, these temperatures suggest that the xenoliths derived from depths of ~70–80 km, which implies that the base of the thermal boundary layer beneath Knippa could have been as thick as ~100 km (taking ~1300 °C to represent the temperature at the base of the thermal boundary layer). The enrichments of the LREEs and LILEs over middle and heavy REEs are inconsistent with fertile asthenosphere or oceanic mantle origin and instead require that these peridotites were cryptically metasomatized sometime after they were formed by melt depletion (as in Fig. 6). One important factor is the depletions in HFSEs relative to the REEs; these negative HFSE anomalies suggest the involvement of fluids during metasomatism and are often taken to imply an arc origin (Hofmann, 1988; Kelemen et al., 1993; Ryerson and Watson, 1987). Similar features have been seen in mantle xenoliths from the Sierra Nevada (Lee, 2005) and Canadian Cordillera (Peslier et al., 2002).

We envision the origin of the geochemical signatures as follows. Melt was originally extracted from these peridotites, resulting in low Ca, Al, and HREE contents and high Mg# and MgO. Based on the depletions in Ca, Al, and HREE contents with respect to an assumed fertile mantle starting composition, we estimate that these peridotites had ~15%–20% melt extracted (using experimental compositions of Walter [Walter et al., 1995, 2003] and parameterizations from pMELTS; Ghiorso and Sack, 1995). Such a melting event should generate much more depletion in LREEs and HFSEs relative to the HREEs (Fig. 5B). Thus, after the original melting event, small degrees of fluids or melts had to be added into the residual peridotite. In Figure 5B, we demonstrate the different effects of mixing melt-depleted peridotites with melts having no arc signature (MORB or ocean-island basalt [OIB]) and melts/fluids with a HFSE depletion. For the REEs, only small amounts of melt/fluid addition (0.5%–2.0%) are needed to match the LREE enrichment levels (note that HREEs remain unaffected). However, only the addition of HFSE-poor melts/fluids can generate the negative HFSE anomalies in the Knippa peridotites. The Knippa peridotites most likely represent fragments of subcontinental lithospheric mantle that were metasomatized by arc-like fluids. In contrast, the relatively flat REE patterns and lack of pronounced HFSE anomalies in samples 01A and 08A suggest metasomatism by silicate melts rather than fluids. These samples were metasomatized a second time (by silicate melts), which overprinted an original arc signature. Alternatively, these samples were never metasomatized by fluids. The metasomatic history of the lithospheric mantle beneath Knippa appears to be heterogeneous. However, what is important here is that many of the xenolith samples preserve an arc or subduction signature, begging the question of when this signature was imparted. Next, we consider the origin of fluid metasomatism in the context of various tectonic scenarios to better understand the relationship between the lithospheric mantle and crustal basement in the area.

When Was the Subduction Signature Imparted?

Tectonic Models

In this section, we discuss several scenarios for the origin of the subduction metasomatic signatures seen in the Knippa xenoliths. Since Knippa is thought to occur on the structural edge of the Laurentian craton (Buffler and Sawyer, 1985; Gao et al., 2008; Hatcher et al., 1989; Keller et al., 1989; Mosher, 1998; Viele and Thomas, 1989), two orogenic events that could have imparted subduction signatures are the Grenvillian and Ouachitan orogenies. We will also discuss the possibility that low-angle subduction of the Farallon plate could have also imparted subduction or fluid signatures. We provide a brief tectonic summary of each of these tectonic episodes and then discuss the tectonic episode that is most likely to have been responsible for the metasomatism seen in the Knippa xenoliths.

Scenario 1: Grenville Orogeny (Proterozoic)

The Grenville orogeny, occurring ca. 1 Ga, is recognized worldwide, and is associated with the formation of the supercontinent Rodinia (e.g., Dalziel, 1991; Hoffman, 1991; Moores, 1991; Rivers, 1997; Tollo et al., 2004; Torsvik et al., 1996). Precambrian lithosphere in Texas is found in the Llano Uplift, ~150 km northeast of Knippa. The main tectonic features in the Grenville province are continental arc magmatism and intense collisional deformation. A seismic study of the Grenville province in Ohio revealed a west-dipping suture, which is evidence for subduction beneath the Laurentian craton (Culotta et al., 1990). In addition, the oldest terrane of the Llano Uplift—the 1366–1232 Ma Valley Spring gneiss—is interpreted to be a Laurentian continental arc terrane based on structural and petrologic relationships (Mosher, 1998). The tectonic features seen in Quebec also indicate that the Laurentian craton was intruded by continental arc magmatism prior to collisional orogenesis (Rivers et al., 1993; Tollo et al., 2004). These observations place a convergent-destructive plate boundary along the southern and eastern margin of Laurentia, recording a progression from continental arc magmatism to arc-continent collision and finally continent-continent collision (Mosher, 1998; Mosher et al., 2008). It has been suggested that the subduction polarity in the Llano area inverted toward the south along an E-W–trending margin sometime before collision (Mosher et al., 2008), but overall NW-vergent subduction affecting a wide area of the continent dominated the Grenvillian event in southern Laurentia and could have metasomatized the mantle in the Knippa region.

Alternatively, the existence of an exotic island arc in the Llano Uplift (Roback, 1996) and the inversion of subduction polarity at the end of the Grenville event toward the south could also imply that the Knippa region was attached to a "southern continent," which served as the overriding plate of a Grenville-aged subduction zone with a southward polarity (S. Mosher, 2009, personal commun.). Under either scenario, the presence of continental arc magmatism in Proterozoic Texas and the general association of the crustal Grenville province with arc magmatism could thus explain the observed fluid-metasomatized signature of the Knippa mantle xenoliths.

Scenario 2: Ouachita Orogeny (Paleozoic)

During the Paleozoic, the closing of the Iapetus and Rheic Oceans assembled the supercontinent of Pangea. Models for the Iapetus and Rheic Oceans are debated, but the following interpretation is preferred: structural evidence for periods of both east- and west-directed subduction have been proposed for the assembly of eastern Laurentia (Hatcher et al., 1989). Plutonic rocks occur throughout the eastern Appalachians, particularly toward the north (Hatcher et al., 1989), but little evidence exists that the subduction regime was actually "continental" in the southern Appalachians. In addition, based on the high burial depths of the Laurentian margin beneath the exotic Avalon terrane in the southeastern Appalachians, it is likely that Laurentia served as the underlying plate along much of the final suture with Gondwana during the Paleozoic orogenies (Keller and Hatcher, 1999). The east-dipping suture of Gondwana to Laurentia following closure of the Rheic Ocean is recognized in both seismic-reflection and magnetic anomaly data, marking a major crustal boundary in Florida (Buffler and Thomas, 1994).

In contrast to the eastern margin, the southern margin of Laurentia appears to have interacted with the Rheic Ocean only because North America rotated clockwise to close the Iapetus (Dalziel, 1997; Murphy and Nance, 2008; Scotese et al., 1990), and it has experienced a more limited accretionary history (Viele and Thomas, 1989). The Rheic Ocean is proposed to have closed primarily beneath Baltica on one side and South America on the other (Murphy et al., 2008). The polarity of subduction has been debated for the Ouachita belt, but several lines of evidence make a compelling argument for south-directed subduction. The Ouachita orogenic belt in southern Laurentia is devoid of arc materials, or volcanic strata of any kind other than fine ash falls (Wickham et al., 1976), while strong evidence exists for long-lived continental arc magmatism on the opposite (Andean) margin (Dalziel et al., 1994) and in Mexico's Acatlàn Complex (Cameron et al., 1992; Jones et al., 1986; McKee et al., 1988). The sedimentary and structural history of the Ouachita belt shows that a deep-water accretionary wedge was thrust over the Laurentian continental shelf and its Proterozoic basement ahead of arc terranes with Gondwanan affinities above south-directed subduction (Poole et al., 2005). Furthermore, the sedimentary package of the Ouachita belt records an increasing influence in time of volcanic source material from the southwest in deep-water shelf sediments, suggesting the approach of an overriding arc from the southwest above south-directed subduction (Mack et al., 1983; Wickham et al., 1976). A geophysical cross section of the Gulf Coast region by Mickus and Keller (1992) recognized a south-dipping suture south of the metamorphic core of the Ouachita belt. The lack of metamorphism in the Ouachita zone is evidence that the suture for the Rheic Ocean in this part of Laurentia was far removed (Nance and Linneman, 2008).

To summarize, most of the geologic and geophysical evidence suggests that the subduction associated with the southern Alleghenian and Ouachita orogenies was directed away from the margin of southern Laurentia; that is, southern Laurentia during this time represented the underthrust plate, not the overriding plate. If so, it would seem unlikely for the subduction-related metasomatic signatures in the Knippa xenoliths to be associated with Paleozoic orogeny.

Scenario 3: Flat Subduction of Farallon Plate during Cenozoic Laramide Orogeny

A third subduction scenario is the flat subduction of the Farallon plate eastward during the Laramide orogeny (74–40 Ma). The low-angle slab may have reached as far east as the Colorado Plateau (Lee, 2005), and so the possibility of the slab reaching even farther east to Knippa should be considered. However, Ar-Ar dates of the Knippa basalts suggest that they erupted well before the apogee of flat subduction (Miggins et al., 2004). Geochemical evidence from arc basalts suggests that dehydration of the slab beneath the arc is highly efficient (>90%) (Shaw et al., 2008), so it is unlikely that much fluid would survive transport as far east as Knippa to cause the observed signature in the Knippa xenoliths.

Additional Discussion on the Origin of the Subduction-Zone Geochemical Signatures

Based on the proposed geometries for the Proterozoic and Paleozoic orogenies described here, we speculate that the observed geochemical signature is best explained by the Proterozoic subduction zone and mantle wedge. This interpretation is consistent with isotopic studies of mantle and lower-crustal xenoliths from the Prairie Creek lamproites in Arkansas, which are contemporary, and which are assumed, on the basis of structural relationships and gravity profiles, to have similar source structural terranes as the Knippa basalts. Osmium (Lambert et al., 1995) and K-Ar (Dunn, 2008) dates of the xenoliths from Prairie Creek point to a lithospheric mantle source with a Proterozoic separation age of 1.2–1.4 Ga and a lower crust with Laurentian affinities and an age of 1.4 Ga. The occurrence of Proterozoic lower-crustal xenoliths is strong evidence that the Ouachita trough is attenuated Proterozoic Laurentian basement and not a remnant ocean basin (Dunn, 2008). These observations and our interpretation of the Knippa xenoliths suggest that lithosphere formed prior to the Grenville collision has been preserved beneath the Gulf Coast despite subsequent orogenies and rifting events, including the latest opening of the Gulf of Mexico. It has been proposed that lithosphere along the Texas-Louisiana coast has been significantly thinned or attenuated (Dunbar and Sawyer, 1987). Rifting may have also removed a large area of Proterozoic basement from the midcontinent region (Thomas, 1991; Thomas and Astini, 1996), which further raises questions about the integrity of the deep lithosphere beneath the Laurentian margin through time. The preservation of Proterozoic mantle lithosphere along Laurentia's southern margin has relevance to the dynamics and process of subcontinental lithospheric mantle stabilization in an orogen, which we discuss next.

Fate of Lithospheric Mantle in an Orogenic Belt

The growth and stabilization of continents have long been thought to be related to convergent margins. For example, along convergent margins, subducting oceanic lithosphere drives juvenile arc magmatism, while relative plate motions accrete island-arc material to the continental margins (Jordan, 1978; Kelemen, 1995; Kelemen et al., 1993; Lee et al., 2007b; Ringwood, 1975; Rudnick, 1995). However, convergent margins also appear to be regions where large-scale convective removal (e.g., "delamination") of the subcontinental lithospheric mantle is thought to occur, as is often depicted in cartoons or invoked to drive postorogenic magmatism, uplift, and recycling of MgO-rich cumulates (Bird, 1979; Houseman et al., 1981; Kay and Kay, 1993; Rudnick, 1995). Postorogenic or anorogenic 1.1–1.0 Ga "A-type" granites occur in the Grenville province (Mosher, 1998; Walker, 1992). Exposure of medium-temperature eclogites in the Llano Uplift (Wilkerson et al., 1988) and deep crustal

exhumation in Quebec (Rivers et al., 1993) suggest exhumation of half the thickness of the orogen. Mosher et al. (2008) suggested that lithospheric delamination may have driven this uplift. Such destruction interferes with the arc-accretion processes that lead to stable, thick, and buoyant cratons.

Many have suggested that after continent-continent collisions, lithospheric mantle in general will be delaminated (Bird, 1979; Corrigan and Hanmer, 1997; Davies and Vonblanckenburg, 1995; Houseman et al., 1981; Turner et al., 1996). However, the preservation of subduction-zone geochemistry in the mantle beneath Grenville-age rocks in southern Laurentia suggests that parts of the original mantle root were not delaminated during the Grenville or Alleghenian orogenies and may have instead been preserved for over 1 b.y.

This conclusion seems somewhat surprising at face value because the Knippa xenoliths are not as refractory as many Archean cratonic mantle peridotites, the densities of which are consequently so low that it is difficult to destabilize them using buoyancy considerations alone. The Mg# values of the Knippa xenoliths are similar to other post-Archean lithospheric mantle, and hence their chemical buoyancies are not likely to be as high as typical cratonic mantle peridotites. Therefore, their preservation suggests that density alone is not controlling the long-term preservation of continental lithospheric mantle. One possibility is rheology. The viscosity of the Laurentian margin could have been high, either because the lithospheric mantle had been dehydrated during partial melting or the lithospheric mantle had already stabilized, cooled, and strengthened (Hirth and Kohlstedt, 1996). The Knippa xenoliths show subduction-related signatures, which imply that the nominally anhydrous minerals (olivine and pyroxenes) may have been rehydrated, and, if so, one would expect much of the lithospheric mantle to have been weakened and possibly removed. The original lithosphere thickness along the southern Laurentian margin could have been at least ~150 km thick based on the presence of diamonds in the Prairie Creek lamproite in Arkansas. The fact that the present lithosphere thickness beneath Knippa is <80 km suggests that the lower half may indeed have been progressively removed. The upper part of the lithosphere, being colder, may have escaped delamination because it was just too cold to deform. This leads us to speculate that continental lithospheric mantle, however it is formed, is relatively resistant to being recycled completely into the mantle, but the mechanism of preservation of such lithosphere still remains elusive.

CONCLUSIONS

Mantle xenoliths erupted through the lithosphere along the Texas coast are characteristic of continental lithosphere and show strong evidence for metasomatism deficient in high field strength elements, suggesting a relationship with arc- or subduction-related fluids. We favor an association of this signature with the Proterozoic Grenville orogeny based on structural relationships and evaluation of tectonic models. The preservation of metasomatized material implies that part of the subcontinental lithospheric mantle remained in place (stable) following orogeny and did not delaminate everywhere.

ACKNOWLEDGMENTS

We thank Julia Morgan for discussions and help in the field. This work was partially supported by the National Science Foundation and Packard grants to Lee.

REFERENCES CITED

Agranier, A., and Lee, C.-T.A., 2007, Quantifying trace element disequilibria in mantle xenoliths and abyssal peridotites: Earth and Planetary Science Letters, v. 257, p. 290–298, doi: 10.1016/j.epsl.2007.02.041.

Bird, P., 1979, Continental delamination and the Colorado Plateau: Journal of Geophysical Research, v. 84, p. 7561–7571.

Brey, G.P., and Köhler, T., 1990, Geothermobarometry in four-phase lherzolites: II. New thermobarometers, and practical assessment of existing thermobarometers: Journal of Petrology, v. 31, p. 1353–1378.

Buffler, R.T., and Sawyer, D.S., 1985, Distribution of crust and early history, Gulf of Mexico Basin: Gulf Coast Association of Geological Societies Transactions, v. 35, p. 333–344.

Buffler, R.T., and Thomas, W.A., 1994, Crustal structure and evolution of the southeastern margin of North America and the Gulf of Mexico Basin, *in* Speed, R.C., ed., Phanerozoic Evolution of North American Continent-Ocean Transitions: Boulder, Geological Society of America, Geology of North America, Decade of North American Geology, Summary Volume to Continent-Ocean Transect Series, p. 219–264.

Byerly, G.R., 1991, Igneous activity, *in* Salvador, A., ed., The Gulf of Mexico Basin: Boulder, Colorado, Geological Society of America, The Geology of North America, v. J, p. 91–108.

Cameron, K.L., Robinson, J.V., Niemeyer, S., Nimz, G.J., Kuentz, D.C., Harmon, R.S., Bohlen, S.R., and Collerson, K.D., 1992, Contrasting styles of pre-Cenozoic and mid-Tertiary crustal evolution in northern Mexico—Evidence from deep crustal xenoliths from La-Olivina: Journal of Geophysical Research–Solid Earth, v. 97, p. 17,353–17,376, doi: 10.1029/92JB01493.

Canil, D., 2004, Mildly incompatible elements in peridotites and the origins of mantle lithosphere: Lithos, v. 77, p. 375–393, doi: 10.1016/j.lithos.2004.04.014.

Condie, K.C., Cox, J., O'Reilly, S.Y., Griffin, W.L., and Kerrich, R., 2004, Distribution of high field strength and rare earth elements in mantle and lower crustal xenoliths from the Southwestern United States: The role of grain-boundary phases: Geochimica et Cosmochimica Acta, v. 68, p. 3919–3942, doi: 10.1016/j.gca.2004.03.025.

Corrigan, D., and Hanmer, S., 1997, Anorthosites and related granitoids in the Grenville orogen: A product of convective thinning of the lithosphere?: Geology, v. 25, p. 61–64, doi: 10.1130/0091-7613(1997)025<0061:AARGIT>2.3.CO;2.

Culotta, R.C., Pratt, T., and Oliver, J., 1990, A tale of two sutures—COCORP's deep seismic surveys of the Grenville province in the eastern U.S. Midcontinent: Geology, v. 18, p. 646–649, doi: 10.1130/0091-7613(1990)018<0646:ATOTSC>2.3.CO;2.

Dalziel, I.W.D., 1991, Pacific margins of Laurentia and East Antarctica–Australia as a conjugate rift pair—Evidence and implications for an Eocambrian supercontinent: Geology, v. 19, p. 598–601, doi: 10.1130/0091-7613(1991)019<0598:PMOLAE>2.3.CO;2.

Dalziel, I.W.D., 1997, Neoproterozoic-Paleozoic geography and tectonics: Review, hypothesis, environmental speculation: Geological Society of America Bulletin, v. 109, p. 16–42, doi: 10.1130/0016-7606(1997)109<0016:ONPGAT>2.3.CO;2.

Dalziel, I.W.D., Dallasalda, L.H., and Gahagan, L.M., 1994, Paleozoic Laurentia-Gondwana interaction and the origin of the Appalachian-Andean mountain system: Geological Society of America Bulletin, v. 106, p. 243–252, doi: 10.1130/0016-7606(1994)106<0243:PLGIAT>2.3.CO;2.

Davies, J.H., and Vonblanckenburg, F., 1995, Slab breakoff—A model of lithosphere detachment and its test in the magmatism and deformation of collisional orogens: Earth and Planetary Science Letters, v. 129, p. 85–102, doi: 10.1016/0012-821X(94)00237-S.

Dunbar, J.A., and Sawyer, D.S., 1987, Implications of continental-crust extension for plate reconstruction—An example from the Gulf of Mexico: Tectonics, v. 6, p. 739–755, doi: 10.1029/TC006i006p00739.

Dunn, D.P., 2008, Arkansas crustal xenoliths: Implications for basement rocks of the northern Gulf Coast, USA: Lithosphere, v. 1, p. 60–64, doi: 10.1130/L10.1.

Eggins, S.M., Rudnick, R.L., and McDonough, W.F., 1998, The composition of peridotites and their minerals: A laser-ablation ICP-MS study: Earth and Planetary Science Letters, v. 154, p. 53–71, doi: 10.1016/S0012-821X(97)00195-7.

Ewing, T.E., and Caran, C.S., 1982, Late Cretaceous volcanism in south and central Texas: Stratigraphic, structural and seismic models: Gulf Coast Association of Geological Societies Transactions, v. 32, p. 137–145.

Flawn, P.T., Goldstein, A., King, P.B., and Weaver, C.E., 1961, The Ouachita System: Austin, Bureau of Economic Geology, University of Texas, 401 p.

Gao, S.S., Liu, K.H., Stern, R.J., Keller, G.R., Hogan, J.P., Pulliam, J., and Anthony, E.Y., 2008, Characteristics of mantle fabrics beneath the south-central United States: Constraints from shear-wave splitting measurements: Geosphere, v. 4, p. 411–417, doi: 10.1130/GES00159.1.

Ghiorso, M.S., and Sack, R.O., 1995, Chemical mass transfer in magmatic processes: IV. A revised and internally consistent thermodynamic model for the interpolation and extrapolation of liquid-solid equilibria in magmatic systems at elevated temperatures and pressures: Contributions to Mineralogy and Petrology, v. 119, p. 197–212, doi: 10.1007/BF00307281.

Griffin, W.R., Stern, R.J., Manton, W.I., Leybourne, M.I., and Bergman, S.C., 2008, Cretaceous extensional focusing of FOZO and FOZO-HIMU derived melts in the Balcones igneous province, Texas: Geological Society of America Abstracts with Programs, v. 40, no. 3, p. 12.

Hatcher, R.D., Jr., 1989, Tectonic synthesis of the U.S. Appalachians, *in* Hatcher, R.D., Jr., Thomas, W.A., and Viele, G.W., eds., The Appalachian-Ouachita Orogen in the United States: Boulder, Colorado, Geological Society of America, The Geology of North America, v. F-2, p. 511–535.

Hatcher, R.D., Jr., Thomas, W.A., and Viele, G.W., 1989, The Appalachian-Ouachita orogen in the United States: Boulder, Colorado, Geological Society of America, The Geology of North America, v. F-2, 767 p.

Hirth, G., and Kohlstedt, D.L., 1996, Water in the oceanic upper mantle: Implications for rheology, melt extraction and the evolution of the lithosphere: Earth and Planetary Science Letters, v. 144, p. 93–108, doi: 10.1016/0012-821X(96)00154-9.

Hoffman, P.F., 1991, Did the breakout of Laurentia turn Gondwanaland inside-out?: Science, v. 252, p. 1409–1412, doi: 10.1126/science.252.5011.1409.

Hofmann, A.W., 1988, Chemical differentiation of the Earth—The relationship between mantle, continental-crust, and oceanic-crust: Earth and Planetary Science Letters, v. 90, p. 297–314, doi: 10.1016/0012-821X(88)90132-X.

Houseman, G.A., McKenzie, D.P., and Molnar, P., 1981, Convective instability of a thickened boundary-layer and its

relevance for the thermal evolution of continental convergent belts: Journal of Geophysical Research, v. 86, p. 6115–6132, doi: 10.1029/JB086iB07p06115.

Jones, N.W., McKee, J.W., and Anderson, T.H., 1986, Pre-Cretaceous igneous rocks in north central Mexico: Geological Society of America Abstracts with Programs, v. 18, p. 649.

Jordan, T.H., 1978, Composition and development of continental tectosphere: Nature, v. 274, p. 544–548, doi: 10.1038/274544a0.

Kay, R.W., and Kay, S.M., 1993, Delamination and delamination magmatism: Tectonophysics, v. 219, p. 177–189, doi: 10.1016/0040-1951(93)90295-U.

Kelemen, P.B., 1995, Genesis of high Mg-number andesites and the continental-crust: Contributions to Mineralogy and Petrology, v. 120, p. 1–19, doi: 10.1007/BF00311004.

Kelemen, P.B., Shimizu, N., and Dunn, T., 1993, Relative depletion of niobium in some arc magmas and the continental-crust—Partitioning of K, Nb, La and Ce during melt/rock reaction in the upper-mantle: Earth and Planetary Science Letters, v. 120, p. 111–134, doi: 10.1016/0012-821X(93)90234-Z.

Keller, G.R., and Hatcher, R.D., Jr., 1999, Some comparisons of the structure and evolution of the southern Appalachian-Ouachita orogen and portions of the Trans-European suture zone region: Tectonophysics, v. 314, p. 43–68, doi: 10.1016/S0040-1951(99)00236-X.

Keller, G.R., Braile, L.W., McMechan, G.A., Thomas, W.A., Harder, S.H., Chang, W.F., and Jardine, W.G., 1989, Paleozoic continent-ocean transition in the Ouachita Mountains imaged from Passcal wide-angle seismic reflection-refraction data: Geology, v. 17, p. 119–122, doi: 10.1130/0091-7613(1989)017<0119:PCOTIT>2.3.CO;2.

Klemme, S., 2004, The influence of Cr on the garnet-spinel transition in the Earth's mantle: Experiments in the system MgO-Cr_2O_3-SiO_2 and thermodynamic modelling: Lithos, v. 77, p. 639–646, doi: 10.1016/j.lithos.2004.03.017.

Lambert, D.D., Shirey, S.B., and Bergman, S.C., 1995, Proterozoic lithospheric mantle source for the Prairie-Creek lamproites—Re-Os and Sm-Nd isotopic evidence: Geology, v. 23, p. 273–276, doi: 10.1130/0091-7613(1995)023<0273:PLMSFT>2.3.CO;2.

Lee, C.-T.A., 2005, Trace element evidence for hydrous metasomatism at the base of the North American lithosphere and possible association with Laramide low-angle subduction: The Journal of Geology, v. 113, p. 673–685, doi: 10.1086/449327.

Lee, C.-T.A., Harbert, A., and Leeman, W.P., 2007a, Extension of lattice strain theory to mineral/mineral rare-earth element partitioning: An approach for assessing disequilibrium and developing internally consistent partition coefficients between olivine, orthopyroxene, clinopyroxene and basaltic melt: Geochimica et Cosmochimica Acta, v. 71, p. 481–496, doi: 10.1016/j.gca.2006.09.014.

Lee, C.-T.A., Morton, D.M., Kistler, R.W., and Baird, A.K., 2007b, Petrology and tectonics of Phanerozoic continent formation: From island arcs to accretion and continental arc magmatism: Earth and Planetary Science Letters, v. 263, p. 370–387, doi: 10.1016/j.epsl.2007.09.025.

Longerich, H.P., Jackson, S.E., and Gunther, D., 1996, Laser ablation inductively coupled plasma mass spectrometric transient signal data acquisition and analyte concentration calculation: Journal of Analytical Atomic Spectrometry, v. 11, p. 899–904, doi: 10.1039/ja9961100899.

Mack, G.H., Thomas, W.A., and Horsey, C.A., 1983, Composition of Carboniferous sandstones and tectonic framework of Southern Appalachian–Ouachita orogen: Journal of Sedimentary Petrology, v. 53, p. 931–946.

McDonough, W.F., and Sun, S.-S., 1995, The composition of the Earth: Chemical Geology, v. 120, p. 223–253.

McKee, J.W., Jones, N.W., and Anderson, T.H., 1988, Las Delicias Basin—A record of late Paleozoic arc volcanism in northeastern Mexico: Geology, v. 16, p. 37–40, doi: 10.1130/0091-7613(1988)016<0037:LDBARO>2.3.CO;2.

Mickus, K.L., and Keller, G.R., 1992, Lithospheric structure of the south-central United States: Geology, v. 20, p. 335–338, doi: 10.1130/0091-7613(1992)020<0335:LSOTSC>2.3.CO;2.

Miggins, D.P.B., Charles, D., and Smith, D.V., 2004, Preliminary $^{40}Ar/^{39}Ar$ Geochronology of Igneous Intrusions from Uvalde County, Texas; Defining a More Precise Eruption History for the Southern Balcones Volcanic Province: U.S. Geological Survey Open-File Report 2004-1031, 31 p.

Miser, H.D., 1934, Relation of Ouachita belt of Paleozoic rocks to oil and gas fields of midcontinent region: American Association of Petroleum Geologists Bulletin, v. 18, p. 1059–1077.

Moores, E.M., 1991, Southwest United–States–East Antarctic (SWEAT) connection—A hypothesis: Geology, v. 19, p. 425–428, doi: 10.1130/0091-7613(1991)019<0425:SUSEAS>2.3.CO;2.

Mosher, S., 1998, Tectonic evolution of the southern Laurentian Grenville orogenic belt: Geological Society of America Bulletin, v. 110, p. 1357–1375, doi: 10.1130/0016-7606(1998)110<1357:TEOTSL>2.3.CO;2.

Mosher, S., Levine, J.S.F., and Carlson, W.D., 2008, Mesoproterozoic plate tectonics: A collisional model for the Grenville-aged orogenic belt in the Llano Uplift, central Texas: Geology, v. 36, p. 55–58, doi: 10.1130/G24049A.1.

Murphy, J.B., and Nance, R.D., 2008, The Pangea conundrum: Geology, v. 36, p. 703–706, doi: 10.1130/G24966A.1.

Murphy, J.B., Nance, R.D., and Anonymous, 2008, Evolution of the Rheic Ocean and the conundrum of Pangea: Geological Society of America Abstracts with Programs, v. 40, p. 75.

Nance, R.D., and Linneman, U., 2008, The Rheic Ocean: Origin, evolution, and significance: GSA Today, v. 18, no. 12, p. 4–12, doi: 10.1130/GSATG24A.1.

Niu, Y.L., 2004, Bulk-rock major and trace element compositions of abyssal peridotites: Implications for mantle melting, melt extraction and post-melting processes beneath Mid-Ocean ridges: Journal of Petrology, v. 45, no. 12, p. 2423–2458, doi: 10.1093/petrology/egh068.

Peslier, A.H., Francis, D., and Ludden, J., 2002, The lithospheric mantle beneath continental margins; melting and melt-rock reaction in Canadian Cordillera xenoliths: Journal of Petrology, v. 43, p. 2013–2047, doi: 10.1093/petrology/43.11.2013.

Pollack, H.N., Hurter, S.J., and Johnson, J.R., 1993, Heat-flow from the Earth's interior—Analysis of the global data set: Reviews of Geophysics, v. 31, p. 267–280, doi: 10.1029/93RG01249.

Poole, F.G., Perry, W.J., Jr., Madrid, R.J., and Amaya-Martinez, R., 2005, Tectonic synthesis of the Ouachita-Marathon-Sonora orogenic margin of southern Laurentia: Stratigraphic and structural implications for timing of deformational events and plate tectonic model, *in* Anderson, T.H., Nourse, J.A., McKee, J.W., and Steiner, M.B., eds., The Mojave-Sonora Megashear Hypothesis: Development, Assessment, and Alternatives: Geological Society of America Special Paper 393, p. 543–596, doi: 10.1130/0-8137-2393-0.543.

Ringwood, A.E., 1975, Composition and Petrology of the Earth's Mantle: New York, McGraw-Hill, 617 p.

Rivers, T., 1997, Lithotectonic elements of the Grenville Province: Review and tectonic implications: Precambrian Research, v. 86, p. 117–154, doi: 10.1016/S0301-9268(97)00038-7.

Rivers, T., Vangool, J.A.M., and Connelly, J.N., 1993, Contrasting tectonic styles in the northern Grenville Province—Implications for the dynamics of orogenic fronts: Geology, v. 21, p. 1127–1130, doi: 10.1130/0091-7613(1993)021<1127:CTSITN>2.3.CO;2.

Roback, R.C., 1996, Characterization and tectonic evolution of a Mesoproterozoic island arc in the southern Grenville orogen, Llano Uplift, central Texas: Tectonophysics, v. 265, no. 1–2, p. 29–52, doi: 10.1016/S0040-1951(96)00145-X.

Rudnick, R.L., 1995, Making continental crust: Nature, v. 378, p. 571–578, doi: 10.1038/378571a0.

Ryerson, F.J., and Watson, E.B., 1987, Rutile saturation in magmas—Implications for Ti-Nb-Ta depletion in island-arc basalts: Earth and Planetary Science Letters, v. 86, p. 225–239, doi: 10.1016/0012-821X(87)90223-8.

Scotese, C.R., Van der Voo, R., Mueller, R.D., and McKerrow, W.S., 1990, Phanerozoic plate tectonic reconstructions; results of the PALEOMAP project: Geological Society of America Abstracts with Programs, v. 22, p. 229–230.

Shaw, A.M., Hauri, E.H., Fischer, T.P., Hilton, D.R., and Kelley, K.A., 2008, Hydrogen isotopes in Mariana arc melt inclusions: Implications for subduction dehydration and the deep-Earth water cycle: Earth and Planetary Science Letters, v. 275, p. 138–145, doi: 10.1016/j.epsl.2008.08.015.

Smith, D.V., McDougal, R.R., Smith, B.D., and Blome, C.D., 2008, Distribution of Igneous Rocks in Medina and Uvalde Counties, Texas, as Inferred from Aeromagnetic Data: U.S. Geological Survey Scientific Investigations Report 2007-5191, 12 p., one plate, scale 1:250,000.

Smith, D.V.G., Smith, B.D., Blome, C.D., Pierce, H.A., and Lambert, R.B., 2001, Cretaceous volcanic intrusives in the Edwards Aquifer, Texas, as identified from a high-resolution aeromagnetic survey: Geological Society of America Abstracts with Programs, v. 33, p. 298, paper 127-0.

Spencer, A.B., 1969, Alkalic igneous rocks of Balcones province, Texas: Journal of Petrology, v. 10, p. 272–306.

Thomas, W.A., 1991, The Appalachian-Ouachita rifted margin of southeastern North America: Geological Society of America Bulletin, v. 103, p. 415–431, doi: 10.1130/0016-7606(1991)103<0415:TAORMO>2.3.CO;2.

Thomas, W.A., and Astini, R.A., 1996, The Argentine Precordillera: A traveler from the Ouachita Embayment of North American Laurentia: Science, v. 273, p. 752–757, doi: 10.1126/science.273.5276.752.

Tollo, R.P., Corriveau, L., McLelland, J., and Bartholomew, M.J., 2004, Proterozoic tectonic evolution of the Grenville orogen in North America: An introduction, *in* Tollo, R.P., McLelland, J., Corriveau, L., and Bartholomew, M.J., eds., Proterozoic Tectonic Evolution of the Grenville Orogen in North America: Geological Society of America Memoir 197, p. 1–18, doi: 10.1130/0-8137-1197-5.1.

Torsvik, T.H., Smethurst, M.A., Meert, J.G., Van der Voo, R., McKerrow, W.S., Brasier, M.D., Sturt, B.A., and Walderhaug, H.J., 1996, Continental break-up and collision in the Neoproterozoic and Palaeozoic—A tale of Baltica and Laurentia: Earth-Science Reviews, v. 40, p. 229–258, doi: 10.1016/0012-8252(96)00008-6.

Turner, S.P., Kelley, S.P., VandenBerg, A.H.M., Foden, J.D., Sandiford, M., and Flottmann, T., 1996, Source of the Lachlan fold belt flysch linked to convective removal of the lithospheric mantle and rapid exhumation of the Delamerian-Ross fold belt: Geology, v. 24, p. 941–944, doi: 10.1130/0091-7613(1996)024<0941:SOTLFB>2.3.CO;2.

Viele, G.W., and Thomas, W.A., 1989, Tectonic synthesis of the Ouachita orogenic belt, *in* The Appalachian-Ouachita Orogen in the United States, *in* Hatcher, R.D., Jr., Thomas, W.A., and Viele, G.W., eds., The Appalachian-Ouachita Orogen in the United States: Boulder, Colorado, Geological Society of America, The Geology of North America, v. F-2, p. 695–728.

Walker, N., 1992, Middle Proterozoic geologic evolution of Llano Uplift, Texas—Evidence from U-Pb zircon geochronometry: Geological Society of America Bulletin, v. 104, p. 494–504, doi: 10.1130/0016-7606(1992)104<0494:MPGEOL>2.3.CO;2.

Walter, M.J., Sisson, T.W., and Presnall, D.C., 1995, A mass proportion method for calculating melting reactions and application to melting of model upper mantle lherzolite: Earth and Planetary Science Letters, v. 135, p. 77–90, doi: 10.1016/0012-821X(95)00148-6.

Walter, M.J., Heinrich, D.H., and Karl, K.T., 2003, Melt extraction and compositional variability in mantle lithosphere, *in* Carlson, R.W., ed., Treatise on Geochemistry: Oxford, Pergamon, v. 2, p. 363–394.

Wells, P.R.A., 1977, Pyroxene thermometry in simple and complex systems: Contributions to Mineralogy and Petrology, v. 62, p. 129–139, doi: 10.1007/BF00372872.

Wickham, J., Roeder, D., and Briggs, G., 1976, Plate tectonics models for Ouachita foldbelt: Geology, v. 4, p. 173–176, doi: 10.1130/0091-7613(1976)4<173:PTMFTO>2.0.CO;2.

Wilkerson, A., Carlson William, D., and Smith, D., 1988, High-pressure metamorphism during the Llano orogeny inferred from Proterozoic eclogite remnants: Geology, v. 16, p. 391–394, doi: 10.1130/0091-7613(1988)016<0391:HPMDTL>2.3.CO;2.

Woodruff, C.M., and Foley, D., 1985, Thermal regimes of Balcones-Ouachita trend: Central Texas: American Association of Petroleum Geologists Bulletin, v. 69, p. 1431.

Yaxley, G.M., Crawford, A.J., and Green, D.H., 1991, Evidence for carbonatite metasomatism in spinel peridotite xenoliths from western Victoria, Australia: Earth and Planetary Science Letters, v. 107, p. 305–317, doi: 10.1016/0012-821X(91)90078-V.

MANUSCRIPT RECEIVED 10 JULY 2009
MANUSCRIPT ACCEPTED 25 AUGUST 2009

Printed in the USA